



## Generation of heat and stress during the cure of polymers used in fiber composites

Christian Heinrich <sup>a</sup>, Michael Aldridge <sup>b</sup>, Alan S. Wineman <sup>c</sup>, John Kieffer <sup>b</sup>, Anthony M. Waas <sup>a,\*</sup>, Khaled W. Shahwan <sup>d,e</sup>

<sup>a</sup> Department of Aerospace Engineering, University of Michigan, Ann Arbor, MI 48109, United States

<sup>b</sup> Department of Materials Science and Engineering, University of Michigan, Ann Arbor, MI 48109, United States

<sup>c</sup> Department of Mechanical Engineering, University of Michigan, Ann Arbor, MI 48109, United States

<sup>d</sup> Automotive Composites Consortium – ACC, and Predictive Technology Development and Composites Crash Energy Management Group (ACC100), USCAR, Southfield, MI 48075, United States

<sup>e</sup> Chrysler Technology Center, Chrysler Group LLC, Auburn Hills, MI 48326-2757, United States

### ARTICLE INFO

#### Article history:

Received 27 June 2011

Received in revised form 9 December 2011

Accepted 10 December 2011

Available online 3 February 2012

#### Keywords:

Mechanics

Curing

Polymers

Coupled physics

Stress evolution

Composites

Virtual manufacturing

### ABSTRACT

The modeling of coupled heat generation, cure, evolution of mechanical properties, and stress generation during the solidification of a polymer epoxy is investigated. Heat conduction and cure kinetics are governed by a system of coupled nonlinear partial differential equations. In the special cases of perfect insulators or perfect conductors, the equations are solved in closed form. Otherwise they are solved numerically. The sensitivity of curing time, maximum temperature during cure and curing stresses are discussed with respect to the chemical and thermal parameters and the volume of material that is cured. It is seen that smaller volumes of the same material cure at a fairly uniform rate whereas a sharp increase in the curing rate is obtained as the volume of material to be cured is increased. Subsequently a model is introduced to describe the stress generation during cure. The cure dependent material properties of Epon 862/Epikure 9553 are presented. Finally it is shown that the volume dependency of temperature during cure leads to stresses in an otherwise homogeneous body. Proper knowledge of the post cure stress state is important as this may alter the effective, or in situ, properties of the cured epoxy (Song, Waas, Shahwan, Faruque, & Xiao, 2008; Song, Waas, Shahwan, Faruque, & Xiao, 2009; Song, Waas, Shahwan, Xiao, & Faruque, 2007; Yerramalli & Waas, 2002). In turn, the in situ properties are a crucial ingredient in any subsequent predictive methodology.

© 2011 Elsevier Ltd. All rights reserved.

## 1. Introduction

The increasing demand for more lightweight structures in aerospace, automotive and other applications drives the need for more sophisticated and optimized composite materials and analysis methods to predict their behavior. A typical representative of such composite structures is carbon fiber textile composites with an epoxy matrix. In order to design the material for its intended use, the structural part to be manufactured can be designed with respect to geometrical properties, fiber architecture, thickness and lay-up. Another important aspect is the manufacturing process itself, as this can have an impact on the subsequent part performance during the application of service loads, because the manufacturing process can produce self-equilibrating internal stresses within the material. If the process is modeled and understood properly, then the desired

\* Corresponding author.

E-mail address: [dcw@umich.edu](mailto:dcw@umich.edu) (A.M. Waas).

internal stress state can be “designed” so that subsequent part performance is enhanced. Such an approach has precedent in the manufacturing process of auto-glass, where compressive surface stresses are “built-in” by tailoring the manner by which the cooling process is controlled, as shown in the pioneering work by Lee, Rogers, and Woo (1965). At the same time, it is shown that different cooling rate histories can produce undesired surface tensile stresses, which if present, can accelerate the propagation of surface flaws like cracks, when tensile service loads are experienced.

Manufacturing induced effects have usually been studied in the context of cure induced stresses and potential localized micro-damage during cure. Rabearison, Jochum, and Grandidier (2009) give an example of how spatial gradients in cure develop in a thick carbon epoxy tube and subsequently cause cracks. Following this, they developed a numerical model for curing of an epoxy. They calculate the curing of the epoxy in a glass beaker and conclude that stresses large enough to cause cracks are developed during the curing process. In a similar fashion Corden, Jones, Jones, and Middleton (1998) have developed a curing model to predict the residual stresses in thick resin transfer molded laminated cylinders. They identified chemical shrinkage due to cure as a major contributing mechanism for stress build up as they cured all parts at room temperature. During the experimental validation of the results with different laminate layouts it was noted that interlaminar cracking can occur due to differential shrinkage. Plepys and Farris (1990), noted the creation of cracks during isothermal cure of three-dimensionally constrained epoxy resin in a glass cylinder. Chekanov, Korotkov, Rozenberg, Dzhavadyan, and Bogdanova (1995), have identified different defect types that may occur during the constrained cure of epoxy resins. At high temperature, cohesive defects intersecting the resin were observed, at medium temperatures uneven voids were found and at low temperatures zigzag defects and cohesive smaller defects were seen.

Studies that investigate the curing process of composites are commonly broken down into two parts: chemical reaction, heat generation and heat conduction, and, the evolution of stress and development of structural integrity. In order to understand and optimize the manufacturing process both issues must be understood well. The temperature field is usually modeled using the standard heat equation and Fourier's law. The cure kinetics are usually modeled using a phenomenological model proposed by Kamal (1974). This model has been employed by a variety of studies on the curing kinetics of various epoxy and hardener systems: Shanku, Vaughan, and Roux (1997) and O'Brien et al. (2003), investigated Epon 862 and curing agent W, (Ramakrishnan, Zhu, & Pitchumani, 2000), were concerned with Epon 815/Epicure 3274, and Adolf and Chambers (1997), with Epon 828/DEA and Epon 828/Z. In a similar fashion the cure of other materials can be modeled. Abhilash, Kannan, and Varkey (2010), for example investigated the heat conduction and chemical evolution of rubber at various temperatures experimentally and numerically. They showed that due to low heat conduction gradients in curing rate and temperature will occur.

The evolution of stress during the cure of epoxy is modeled through a variety of approaches. Plepys and Farris (1990) and Plepys, Vradsnos, and Farris (1994) used incremental elasticity to describe the evolution of stresses and elastic properties as a function of cure. They assume that during each time increment, the stress increment is related to the strain increment as a linear isotropic elastic relation with a changing modulus as a function of cure. Bogetti and Gillespie (1992), used a linear mixing rule based on degree of cure, elastic modulus of uncured and fully cured resin moduli and a parameter to quantify stress relaxation and chemical hardening. Another material model often used involves linear viscoelasticity (Adolf & Chambers, 1997; Adolf, Martin, Chambers, Burchett, & Guess, 1998; Lange, Toll, Månsen, & Hult, 1995; White & Hahn, 1992). Here the evolution of the cure dependent (and therefore time dependent) material properties was modeled with the aid of integral constitutive equations found in linear viscoelasticity. A more sophisticated model has been proposed by Adolf and Chambers (2007) using non-linear viscoelasticity. However, such a model with its large amount of parameters also requires extensive validation and experimental investigation (Adolf, Chambers, & Caruthers, 2004).

This paper is concerned with the introduction of a model to understand and quantify the chemical and thermal processes that take place during cure of a thermoset polymer matrix in combination with a model for stress generation introduced earlier by Mei (2000) and Mai, Yee, Wineman, and Xiao (1998).

## 2. Heat conduction and curing

The curing of an epoxy is an exothermic chemical reaction (see for example studies regarding Differential Scanning Calorimetry (DSC) of epoxy, O'Brien et al., 2003; Ramakrishnan et al., 2000; Shanku et al., 1997). The degree of cure is often measured by placing a small sample in a digital scanning calorimeter, maintaining the sample at a constant temperature and measuring the heat that is generated during cure. Denote the heat generated up to time  $t$  by  $H(t)$  and the degree of cure by  $\phi(t)$ , both at time  $t$ . The degree of cure is often defined (Kamal, 1974) by

$$\phi(t) = \frac{H(t)}{H_r}, \quad (1)$$

where  $H_r$  is the total heat that is generated. Thus,  $\phi(t)$  monotonically increases from  $\phi = 0$ , at the uncured state, to  $\phi = 1$ , at the fully cured state. Note that the rate of heat generation per unit mass is

$$r = \frac{d(H_r\phi)}{dt}. \quad (2)$$

**Table 1**

Curing parameters of various epoxy hardener systems.

Reference and material	$H_r$ (J/g)	$m$	$n$	$k_1$	$k_2$
Shanku Epon 862/W	341	0	1	$1.76 \cdot 10^7 \exp\left(\frac{-75000}{RT}\right)/\text{s}$	0
Ramakrishnan Epon 815/Epikure 3274	384	0.25	1.7	0	$4.18^5 \exp\left(\frac{-55920}{RT}\right)/\text{s}$
Obrian and White Epon 862/W	399	0.39	1.67	0	$6488 \exp\left(\frac{-5326K}{RT}\right)/\text{s}$
Adolf Epon 828/DEA	200	–	1.6	$43333 \exp(-66512K/(RT))/\text{s},$ $338 \text{ K} < T < 368 \text{ K}$	$\begin{cases} 9.5 \cdot 10^6 \exp(-66512K/(RT))/\text{s} & \text{if } T < 338 \text{ K} \\ 1.5 \cdot 10^6 \frac{363-T}{(T-273K)^6}/\text{s} & \text{if } 338 \leq T < 363 \\ 0 & \text{if } 363 < T \end{cases}$
Aldridge Epon 862/Epikure 9553	–	0	1	$3.62 \cdot 10^{11} \exp\left(\frac{-88500}{RT}\right)/\text{s}$	0

The curing process is modeled by a kinetics equation of the form

$$\frac{d\phi}{dt} = f(T, \phi), \quad (3)$$

where  $T$  is the temperature and  $f(T, \phi) \geq 0$ . Kamal (1974) has suggested that  $f(T, \phi)$  be given by,

$$f(T, \phi) = (k_1(T) + k_2(T)\phi^m)(1 - \phi)^n, \quad (4)$$

$$k_1(T) = A_1 \exp\left(-\frac{\Delta E_1}{TR}\right), \quad (5)$$

$$k_2(T) = A_2 \exp\left(-\frac{\Delta E_2}{TR}\right), \quad (6)$$

in which  $m$  and  $n$  are constants,  $R$  is the gas constant,  $A_1, A_2$  are frequency like constants and  $\Delta E_1, \Delta E_2$  are activation energies. Choices for  $m, n, k_1(T)$  and  $k_2(T)$  for various epoxy-curing agent systems have appeared in the literature. These values are summarized in Table 1.  $k_1(T)$  and  $k_2(T)$  are fitting constants that are found in the Arrhenius equation, which is used to describe a wide variety of chemical reactions. The exponential portion is related to the probability that a reaction might take place during a collision of atoms. The activation energy describes the energy barrier that needs to be overcome for a reaction to take place. With increasing temperature the kinetic energy of individual atoms increases and it becomes easier to overcome the energetic barrier. In applications, Eq. (3) is used to describe the curing process even when the temperature varies with time (O'Brien et al., 2003).

In a curing structural composite, there is both local heat generation due to curing and heat conduction due to the presence of an external surface or along fibers. This process is governed by the local form of the first law of thermodynamics (Doghri, 2000; Fung, 1994),

$$\rho \frac{de}{dt} = -\frac{\partial q_i}{\partial x_i} + \rho r + \sigma_{ij} \frac{d}{dt} \varepsilon_{ij}, \quad (7)$$

where  $e$  is the internal energy per unit mass,  $\rho$  is the current mass density,  $q_i$  are the components of the heat flux vector,  $r$  is the rate of heat supply per unit mass,  $\sigma_{ij}$  are the stress components and  $\varepsilon_{ij}$  are the components of the infinitesimal strain tensor.

For the applications considered here, the rate of mechanical work,  $\sigma_{ij} de_{ij}/dt$ , is assumed to be negligible and the internal energy is assumed to be proportional to temperature,  $e = cT$ , where  $c$  is the specific heat capacity. The heat flux vector is related to the temperature gradient by the Fourier law of heat conduction,

$$q_i = -\kappa \frac{\partial T}{\partial x_i}, \quad (8)$$

where  $\kappa$  is the thermal conductivity. It is possible that the thermal conductivity depends on the degree of cure and the temperature, i.e.  $\kappa = \kappa(T, \phi)$ . Eq. (7), with (2) and (8) and the stated assumptions becomes,

$$\rho c \frac{\partial T}{\partial t} = \frac{\partial}{\partial x_i} \left( \kappa(\phi, T) \frac{\partial T}{\partial x_i} \right) + \rho H_r \frac{\partial \phi}{\partial t}. \quad (9)$$

Eqs. (3), (4) and (9) form a system of coupled nonlinear partial differential equations for the spatial distribution and time variation of temperature,  $T(x, t)$ , and degree of cure,  $\phi(x, t)$ . (9) is based on energy considerations. However, no further attention is given to the restrictions placed on the curing process due to the second law of thermodynamics. Ideally any study of the process of curing should be written in the context of thermodynamics and include the restrictions placed on the process by the second law of thermodynamics. This however comes at the added expense of specifying a potential with an increased number of free parameters. A full study of the curing process of rubber based on thermodynamical considerations can be found in Kannan and Rajagopal (2011).

### 3. Special cases

It is useful to have analytical solutions to the system of equations (3), (4) and (9). This is shown to be possible in the two limiting cases of a perfect conductor and a perfect insulator.

#### 3.1. Perfect conductor $\kappa \rightarrow \infty$

In this case, (8) implies that  $\partial T/\partial x_i = 0$  and the temperature field in the epoxy is homogeneous. Heat generated by curing is instantaneously conducted. If the body was in an infinite bath of temperature  $T_0$ , then the temperature in the body would be  $T(t) = T_0$  at all times,  $t$ . Let the temperature be fixed. Then the degree of cure is determined by solving (3). When  $f(T, \phi)$  is given by (4),

$$\frac{d\phi}{dt} = (k_1(T) + k_2(T)\phi^m)(1 - \phi)^n. \quad (10)$$

It is convenient to determine the inverse relation  $t = t(\phi)$ , which is possible since  $f(T, \phi) > 0$ . This is obtained from (10),

$$t = \int_0^{\phi(t)} \frac{d\bar{\phi}}{(k_1(T) + k_2(T)\bar{\phi}^m)(1 - \bar{\phi})^n}, \quad (11)$$

where use was made of the initial condition  $\phi = 0$  at  $t = 0$ . Eq. (11) holds also if  $T$  varies with time. In general, the integral in (11) cannot be evaluated analytically for general values of  $m, n, k_1(T)$  and  $k_2(T)$  such as have been experimentally determined, and a numerical method must be used. However, an analytical solution can be obtained in the special case when  $m = n = 1$  and  $T$  is constant in time. Then,

$$t = \frac{1}{k_1 + k_2} \ln \left( \frac{k_2\phi(t) + k_1}{k_1(1 - \phi(t))} \right). \quad (12)$$

This can be inverted to give

$$\phi(t) = \frac{k_1[\exp(\{k_1 + k_2\}t) - 1]}{k_2 + k_1 \exp(\{k_1 + k_2\}t)}, \quad (13)$$

where the arguments of  $k_1$  and  $k_2$  have been suppressed. Note that  $k_1 > 0$  and  $k_2 > 0$  and as  $t \rightarrow \infty$ ,  $\phi \rightarrow 1$ . The rise time depends on  $k_1$  and  $k_2$ .

#### 3.2. Perfect insulator $\kappa \rightarrow 0$

In this case, there is no heat conduction. Heat generated by curing does not conduct away. The temperature field is uniform and its time dependence is determined from (9), which reduces to

$$\rho c \frac{\partial T}{\partial t} = \rho H_r \frac{\partial \phi}{\partial t}. \quad (14)$$

If curing begins at a uniform temperature  $T = T_0$ , then

**Table 2**  
Thermal properties.

Property	Unit	Material	Value	Reference
Density $\rho$	kg/m <sup>3</sup>	Epon862/Epikure3234	1230	Hexion Specialty Chemicals, Inc.
		Current study	1200	
Specific heat $c_p$	J/kg/°C	Generic epoxy	1200@109°C	Garnier and Sommier (2002)
		Epon862/W	1000	Li et al. (2001)
		Bisphenol F/HHPA	1150@23°C	Bujard et al. (1994)
Heat of reaction	J/kg	Current study	1200	
		Epon862/W	399,000 ± 14,000	O'Brien et al. (2003)
		Epon862/W	395,000	Shanku et al. (1997)
		Epon862/W	200,000	Li et al. (2001)
		Epon862/Epikure3234	121,600 ± 6400	Wu and Chung (2004)
		Current study	227,000	
Thermal conductivity $\kappa$	W/m/K	Epon862 resin	0.15–0.20	Varshney et al. (2008)
		DETDA	0.13–0.21	Varshney et al. (2008)
		Epon862/DETDA	0.13–0.30	Varshney et al. (2008)
		Epon862/W	0.195	Ganguli et al. (2008)
		Bisphenol F/HHPA	0.2	Bujard et al. (1994)
		Current study	0.2	

$$T(t) = \frac{H_r}{c} \phi(t) + T_0. \quad (15)$$

Thus, in a poor heat conductor such as an epoxy, the change in temperature is proportional to the change in degree of cure. The overall change in temperature is equivalent to the heat that can be produced during the curing process, divided by the specific heat of the material. It is useful to provide a numerical example using (15). The total heat during curing is about 227 kJ/kg (see Table 2). For Epon 862,  $c = 1.2 \text{ kJ}/(\text{kg K})$ . The temperature rise when fully cured ( $\phi = 1$ ) is then  $T(t) - T_0 = \frac{H_r}{c} = 189 \text{ K}$ . It should be emphasized that this temperature rise only applies to the idealized limit of  $\kappa = 0$  of a perfect insulator.

As in the case of the perfect conductor, it is convenient to first determine the inverse relation  $t = t(\phi)$ . This is given by (11) with  $T$  determined using (15),

$$t = \int_0^{\phi(t)} \frac{d\phi}{(k_1 \left( \frac{H_r}{c} \bar{\phi} + T_0 \right) + k_2 \left( \frac{H_r}{c} \bar{\phi} + T_0 \right) \bar{\phi}^m) (1 - \bar{\phi})^n}. \quad (16)$$

The integral can be numerically evaluated and a plot of  $\phi$  vs.  $t$  can be constructed. A comparison of degree of cure vs. time for the perfect insulator and perfect conductor for Epon 862/9556 and Epon 815/3274 is provided in Fig. 1.

#### 4. Curing of Epon 862/Epikure 9553

Experimental data has been obtained for the degree of cure as a function of time for Epon 862 and Epikure 9553 using Raman light scattering (RLS) (Chike, Myrick, Lyon, & Angel, 1993; Merad et al., 2009). The measurements were taken through isothermal cure cycles at 295 K (22 °C), 303 K (30 °C), 313 K (40 °C) and 323 K (50 °C). The experimental data was scaled such that upon saturation of the curing reaction the final curing value approached 1 to allow for easy comparison with other curing models presented in the literature. The data obtained using Raman light scattering is based on tracking intensities of atomic bond vibrations associated with structural moieties that participate in the polymerization and cross-linking reactions. The intensities of the corresponding spectral bands are directly proportional to the concentrations of these moieties, and hence, allows to quantitatively assess the degree of cure.

The experimental data was curve fitted using a non-linear least squares approach. Two different models were considered. In one case all parameters in (4) were free to vary. In the other case only  $A_1$  and  $\Delta E_1$  were free to vary. The other parameters were set to  $n = 1$ , and  $A_2 = \Delta E_2 = m = 0$ . The result of only two variables being free is shown in Fig. 2. For simplicity, in future discussions the model using only the two fitting constants  $\Delta E_1$  and  $A_1$  will be used. The experimental data indicate that curing temperature and time to full cure are related in a very non-linear fashion. The curing time varies from 40,000 s (about 11 h) at 22 °C and 12,000 s (3.3 h) at 30 °C to 3600 s (1 h) at 40 °C and only about 1800 s (1/2 h) at 50 °C. Fig. 3 shows a fit of the experimental data where  $A_2$ ,  $\Delta E_2$ ,  $m$  and  $n$  are parameters of the model.

#### 5. Comparison of different models

Several authors have investigated the curing behavior of Epon with different curing agents. Shanku et al. (1997) and O'Brien et al. (2003) investigated Epon 862 (bisphenol F epoxide) with curing agent W (diethyloluene diamine). Adolf and

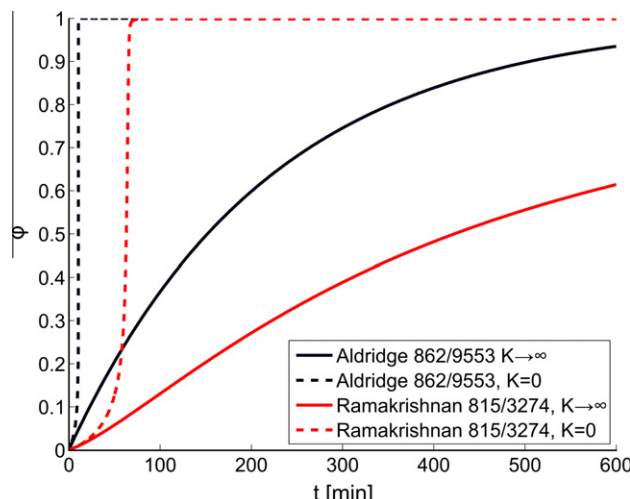
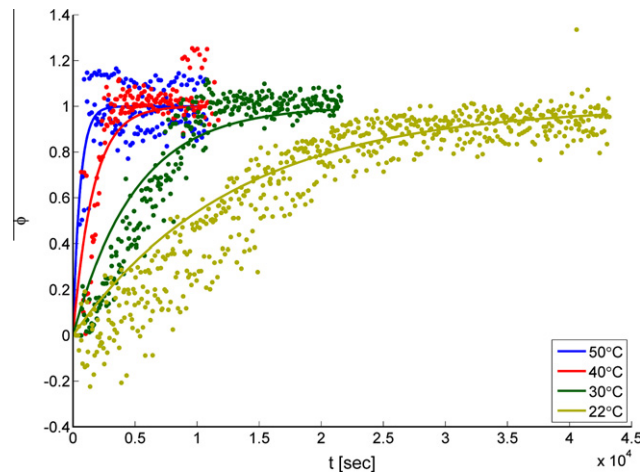
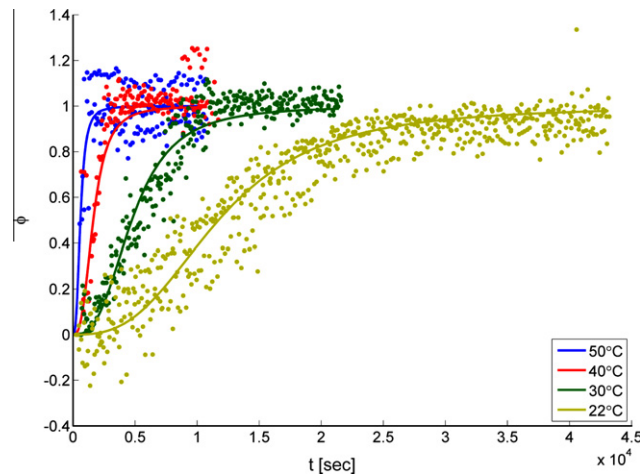


Fig. 1. Comparison  $K = 0$  and  $K \rightarrow \infty$ .



**Fig. 2.** Experimental data and curve fit for isothermal cure.  $A_1$  and  $\Delta E_1$  are parameters to the curing model.  $A_1 = 3.62 \cdot 10^{11} \text{ s}^{-1}$ ,  $\Delta E_1 = 8.854 \cdot 10^4 \text{ J}$ ,  $n = 1$ ,  $m = A_2 = \Delta E_2 = 0$



**Fig. 3.** Experimental data and curve fit for isothermal cure.  $A_2$ ,  $\Delta E_3$ ,  $m$ ,  $n$  are parameters to the curing model.  $A_1 = 0 = \Delta E_1 = 0 \text{ J}$ ,  $A_2 = 1.92 \cdot 10^{11} \text{ s}^{-1}$ ,  $\Delta E_2 = 8.415 \cdot 10^4 \text{ J}$ ,  $m = 0.66$ ,  $n = 1.33$ .

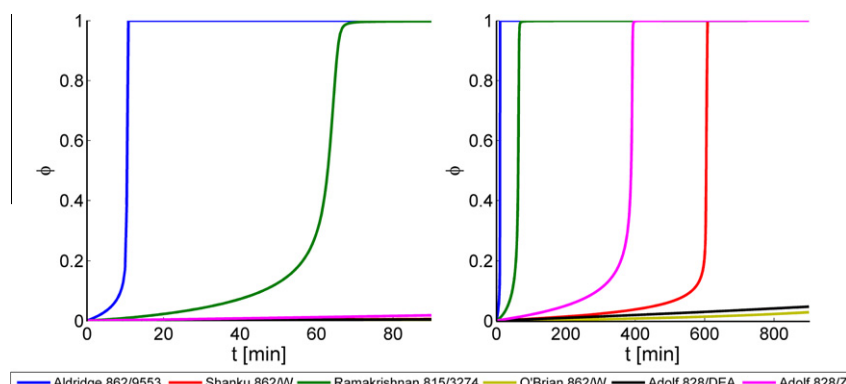


**Fig. 4.** Comparison of different curing models for a perfect insulator,  $T_0 = 295 \text{ K}$ .

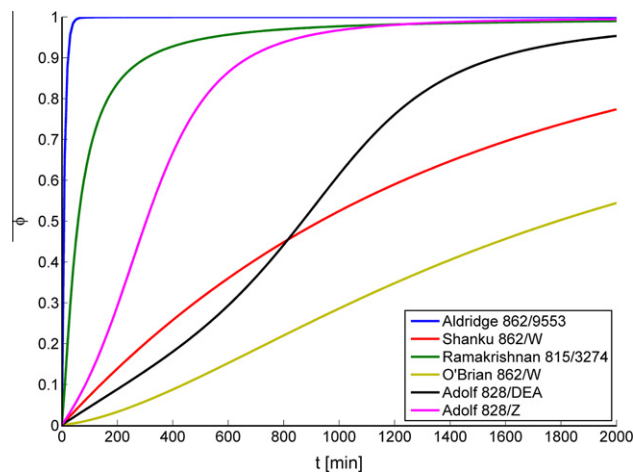


Fig. 5. Comparison of different curing models for a perfect conductor,  $T_0 = 323$  K (50 °C).

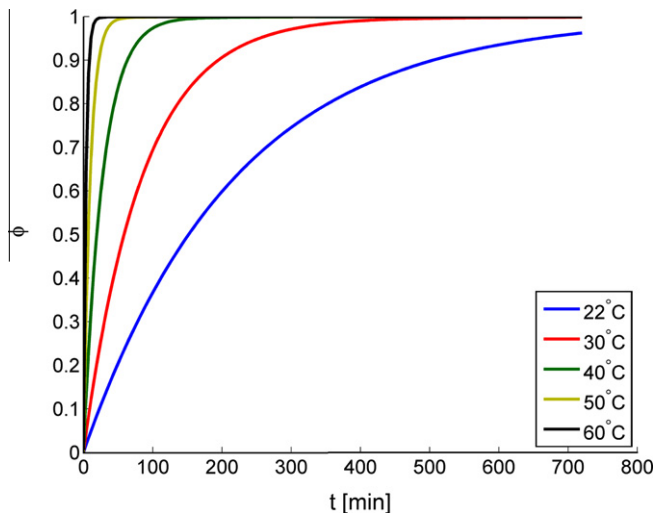


Fig. 6. Degree of cure vs. time for perfect conductor and Epon 862/Epicure 9553 at different boundary temperatures.

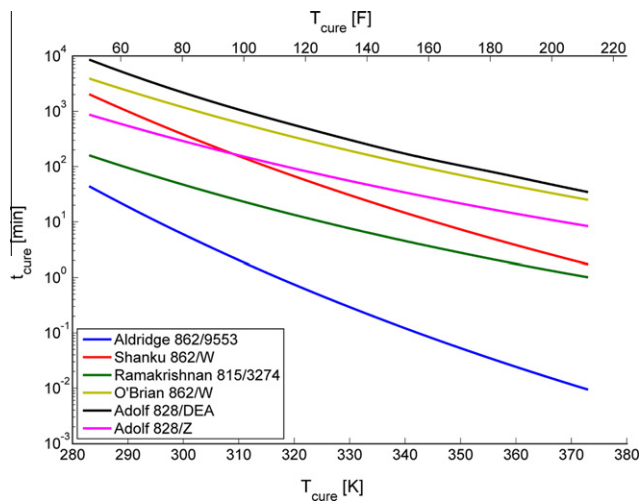
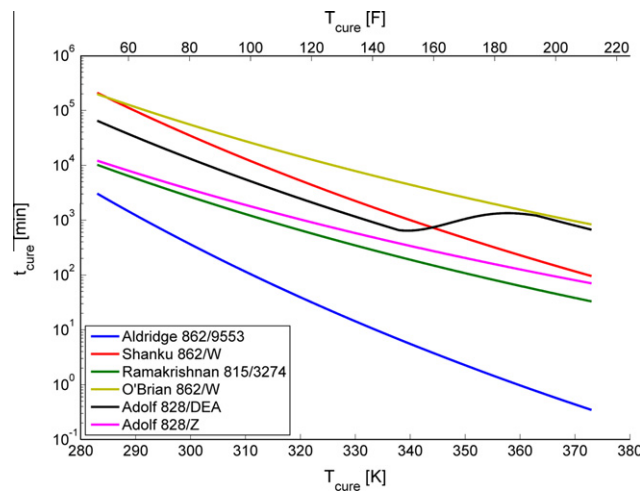


Fig. 7. Time to 95% cure as function of initial temperature, perfect insulator.



**Fig. 8.** Time to 95% cure as function of curing temperature, perfect conductor.

Chambers (1997) were concerned with Epon 828 (bisphenol A based) with curing agent DEA (diethanolamine) and Z (mixture of aromatic amines). Ramakrishnan et al. (2000) obtained data for Epon 815 (bisphenol A based) with curing agent Epikure 3274. They reported values for  $m$  and  $n$  in (4) and expressions for  $k_1(T)$  and  $k_2(T)$  in (5) and (6) for the systems that were investigated. This information is summarized in Table 1.

These values were used in (13) and (16) to determine the degree of cure vs. time for the cases of a perfect conductor and a perfect insulator. As can be seen in Figs. 4–8, the curing reaction predicted by the various models is quite different, not only among different materials, but also within the same epoxy system investigated by different authors.

Fig. 4 shows the degree of cure vs. time for a perfect insulator with an initial temperature of  $T_0 = 295$  K (22 °C). The temperature is proportional to the degree of cure as stated in Eq. (15). Initially,  $\phi = 0$  and the rate of cure is very small. With increasing temperature the rate of cure rises, a self accelerating effect sets in. The heat stays where it is generated which causes the temperature to rise which in turn causes more heat to be released in a shorter time. It is seen that there is a narrow time interval during which the temperature can rise very rapidly. The time when this interval occurs depends strongly on the parameters in  $k_1$  and  $k_2$ . Epon 862/Epikure 9553 and Epon 815/Epikure 3274 cure significantly faster than the other epoxy system considered in Fig. 4. The degree of cure of Epon 862/W and Epon 828 stays close to zero during the time interval shown in Fig. 4.

Fig. 5 shows the degree of cure vs. time for a perfect conductor. The curing reaction is significantly slower. The self accelerating effect cannot be observed since the temperature is fixed. As can be seen from Eq. (10), as  $\phi \rightarrow 1$ ,  $d\phi/dt \rightarrow 0$ , so that the degree of cure asymptotically approaches one. It should be noted that among all epoxy systems that are considered, Epon 862/9553 is by far the most reactive.

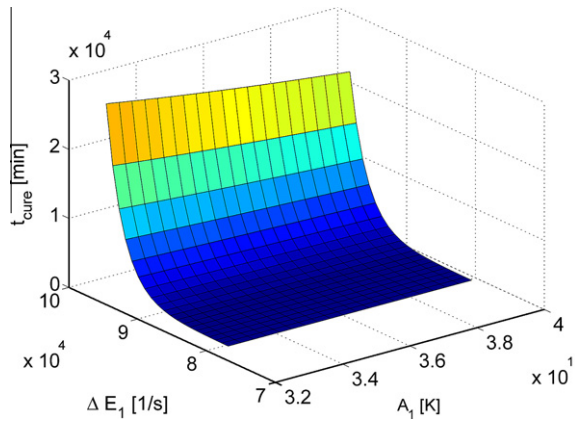
Fig. 6 shows the degree of cure vs. time for a perfect conductor using the material parameters of Epon 862/Epikure 9553 at different boundary temperatures. The degree of cure occurs faster at higher temperatures. Since complete cure,  $\phi = 1$ , is approached asymptotically, a curing time  $t_{cure}$  is defined to be the time corresponding to  $\phi = 0.95$ .

Fig. 7 shows how curing time and initial temperature are related for a perfect insulator. The curing time decreases in an exponential fashion. Between an initial temperature of 283 K (10 °C) and 373 K (100 °C) the curing time drops by two to three orders of magnitude. Epon 862/Epikure 9553 cures the fastest, followed by Epon 815/Epikure 3274. There is a noticeable difference in the predicted curing behavior of Epon 862 between O'Brien et al. (2003) and Shanku et al. (1997). One reason for this might be, that the values of O'Brien and White were measured at a higher temperature level, than the measurements by Shanku et al.

Fig. 8 shows curing time vs. epoxy temperature for a perfect conductor (isothermal conditions). As expected the curing time is significantly higher compared to the perfect insulator. Curing temperature and time are again related in an exponential manner and between 283 K and 373 K the curing time decreases by about two orders of magnitude. Between 338 K and 360 K Epon 828/DEA shows an unexpected behavior with the curing time increasing with temperature. This might be attributed to the piecewise definition of  $k_2$  as given in Table 1.

## 6. Sensitivity analysis

A question arises as to the sensitivity of the results in Figs. 4–8 to the model parameters, namely  $A_1$ ,  $\Delta E_1$ ,  $A_2$ ,  $\Delta E_2$  and  $H_r$ . This is investigated for the perfect conductor and perfect insulator.  $H_r$  does not have any effect in the case of a perfect conductor. In the case of the perfect insulator, a change in  $H_r$  has a scaling effect, as seen in Eq. (15). The sensitivity with respect to the activation energy  $\Delta E_1$  and frequency parameter  $A_1$  for the epoxy system of interest has been investigated here for a perfect conductor and perfect insulator.



**Fig. 9.** Time to 95% cure for different  $A_1$  and  $\Delta E_1$ , perfect conductor,  $T_0 = 295$  K.

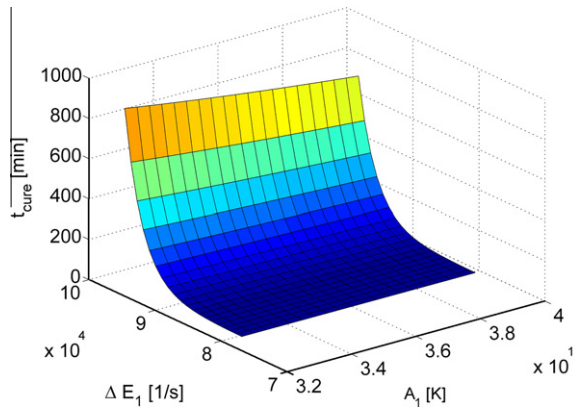


**Fig. 10.** Time to 95% cure for different  $A_1$  and  $\Delta E_1$ , perfect conductor,  $T_0 = 323$  K.

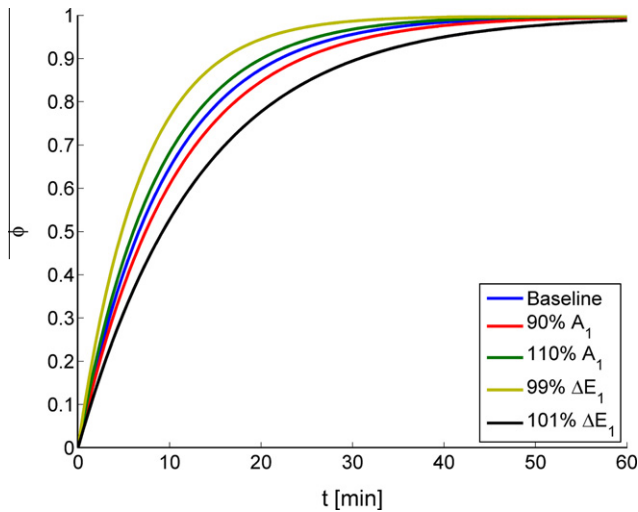


**Fig. 11.** Time to 95% cure for different  $A_1$  and  $\Delta E_1$ , perfect conductor,  $T_0 = 323$  K.

**Fig. 9** shows  $t_{\text{cure}}$  as a function of  $A_1$  and  $\Delta E_1$  for  $T_0 = 295$  K (22 °C) for the perfect conductor and **Fig. 10** shows the same for  $T_0 = 323$  K (50 °C). In both cases, an increase in the frequency parameter  $A_1$  causes a linear decrease in curing time. An increase in the activation energy causes an exponential like increase in the time it takes to cure. This is expected. As seen from Eqs. (5) and (6), an increase in  $\Delta E_1$  has the same effect as decreasing the temperature.

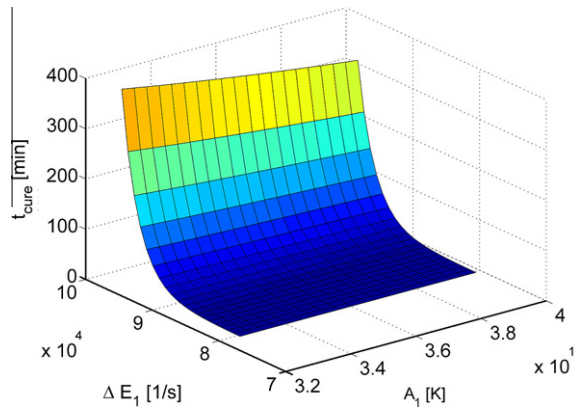


**Fig. 12.** Time to 95% cure for different  $A_1$  and  $\Delta E_1$ , perfect insulator,  $T_0 = 295$  K.

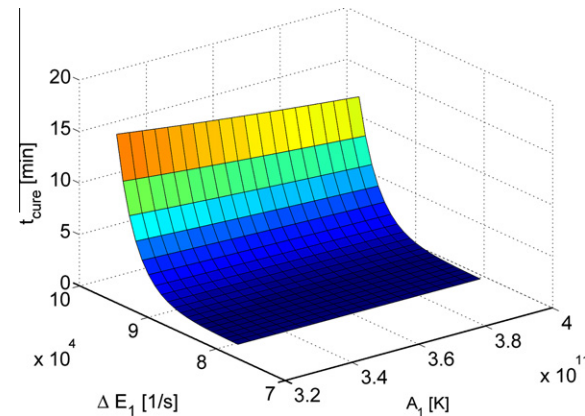


**Fig. 13.** Time to 95% cure for different  $A_1$  and  $\Delta E_1$ , perfect insulator,  $T_0 = 323$  K.

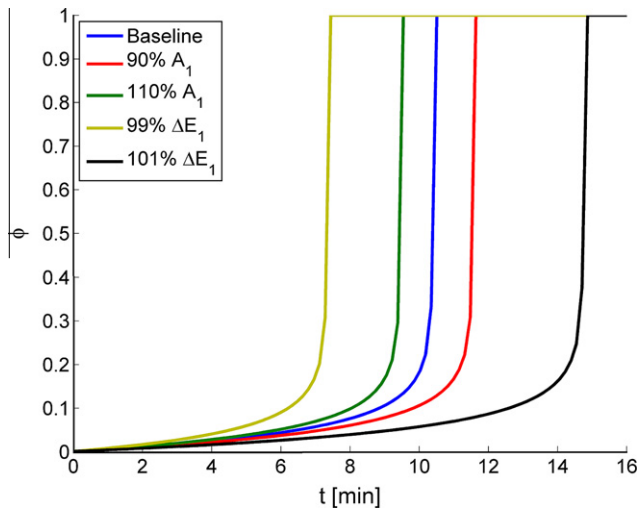


**Fig. 14.** Time to 95% cure for different  $A_1$  and  $\Delta E_1$ , perfect insulator,  $T_0 = 295$  K.

Fig. 11 shows cure histories for a boundary temperature of 323 K with some deviation from the values given by the model. All the histories studied show similar behavior, with a faster curing for higher frequency parameter,  $A_1$ , and lower activation energy.

In Fig. 12, the dependency of the curing time on  $A_1$  and  $\Delta E_1$  is shown for Epon 862/Epikure 9553 and a perfect insulator at 295 K. Fig. 13 shows the same at 323 K. The results are similar to the ones that can be found for the perfect conductor: an

increase in frequency parameter causes the curing time to get smaller in a linear fashion, whereas an increase in the activation energy causes the curing time to increase in an exponential manner. Fig. 14 shows  $\phi$  vs.  $t$ , for the baseline case and some deviation of the model parameters. The initial temperature is 295 K. The curves are similar and compress along the time axis for higher  $A_1$  and lower  $\Delta E_1$ .

## 7. Radial heat generation and conduction in a solid cylinder

Consider an infinitely long circular cylinder of radius  $R_0$  that is filled with epoxy at  $t = 0$ . The cylinder wall is maintained at a constant ambient temperature  $T_{BC}$  while the epoxy cures. The degree of cure and temperature vary with radius and time, i.e.  $\phi = \phi(r, t)$  and  $T = T(r, t)$ . It will be assumed that the thermal conductivity, density and heat of reaction are constants. Some of these assumptions are violated to some degree in reality. During the cure of the epoxy-hardener system, the epoxy will change size due to chemical shrinkage and thermal expansion. However this volume change is on the order of a few percent. There is no experimental data available on the dependency of thermal conductivity on the degree of cure. The results of the molecular dynamics study by Varshney, Patnaik, Roy, and Farmer (2008) point to either a constant thermal conductivity or a lower thermal conductivity of the uncured epoxy-hardener mixture. In the future the thermal conductivity of the fully cured system will be used, which may be seen as an upper bound. Shanku et al. (1997) confirm, that the heat of reaction of Epon 862/W is independent of the heating rate. With these assumption,  $\phi = \phi(r, t)$  and  $T = T(r, t)$  satisfy the nonlinear coupled system of equations,

$$\frac{\partial\phi}{\partial t} = (k_1(T) + k_2(T)\phi^m)(1 - \phi)^n, \quad (17)$$

$$\frac{\partial T}{\partial t} = \frac{\kappa}{\rho c} \left( \frac{\partial^2 T}{\partial r^2} + \frac{1}{r} \frac{\partial T}{\partial r} \right) + \frac{H_r}{c} \frac{\partial \phi}{\partial t}, \quad (18)$$

in which  $k_1(T)$  and  $k_2(T)$  are defined in (5) and (6). The initial conditions are

$$\phi(r, 0) = 0, \quad T(r, 0) = T_i, \quad 0 \leq r \leq R_0. \quad (19)$$

The boundary conditions are that there is no heat flow at the centerline and the outer wall is maintained at a fixed temperature:

$$\frac{\partial T}{\partial r}(0, t) = 0, \quad T(R_0, t) = T_{BC}. \quad (20)$$

As it does not appear possible to solve the system of equations (17) and (18) by analytical methods, they are solved numerically, using a finite differences method and Matlab® (Mathworks, 2009). Choices for values of  $\rho$ ,  $c$ ,  $\kappa$  and  $H_r$  are summarized in Table 2. Numerical results that illustrate the phenomena have been obtained using the data for Epon 862/ Epikure 9553. Initially, when placed in the cylinder, the epoxy is at room temperature  $T_i = 295$  K (22 °C). The outside wall of the cylinder is  $T_{BC} = 323$  K, as one might find in a heated mold or oven. Figs. 15 and 16 show results for  $R_0 = 1$  mm.

As shown in Fig. 15, the temperature in the entire sample rapidly increases from room temperature to the boundary temperature. It overshoots by a small amount due to the heat that is generated during the curing process, but the temperature is

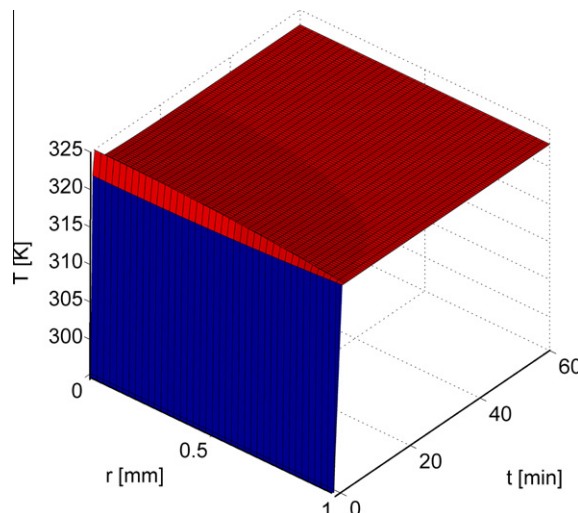


**Fig. 15.** Temperature development,  $R_0 = 1$  mm,  $T_{ini} = 295$  K,  $T_{BC} = 323$  K.

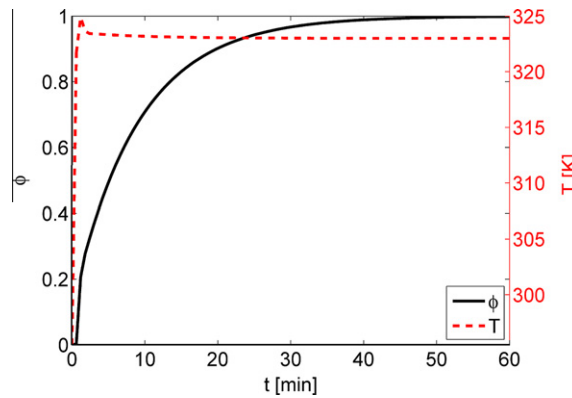


**Fig. 16.** Cure and temperature at midline,  $R_0 = 1 \text{ mm}$ ,  $T_{ini} = 295 \text{ K}$ ,  $T_{BC} = 323 \text{ K}$ .

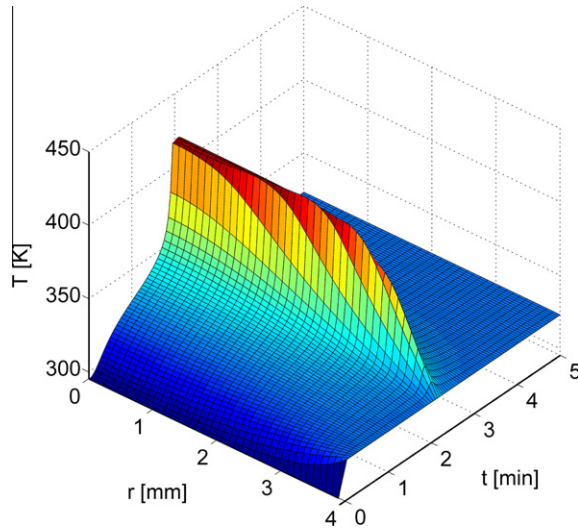


**Fig. 17.** Temperature development,  $R_0 = 4 \text{ mm}$ ,  $T_{ini} = 295 \text{ K}$ ,  $T_{BC} = 323 \text{ K}$ .

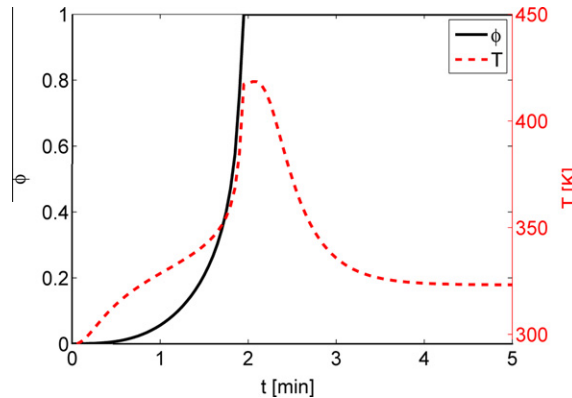


**Fig. 18.** Cure and temperature at midline,  $R_0 = 4 \text{ mm}$ ,  $T_{ini} = 295 \text{ K}$ ,  $T_{BC} = 323 \text{ K}$ .

largely dominated by the boundary temperature. Heat conduction is rapid compared to heat generation. Fig. 16 shows the temperature and degree of cure vs. time at the centerline  $r = 0$ .

A different picture is revealed, when looking at the same example but changing the size of the cylinder to  $R_0 = 4 \text{ mm}$ . Fig. 17 shows  $T(r,t)$  for the entire cylinder. Fig. 18 shows temperature and degree of cure vs.  $t$  at the centerline  $r = 0$ . The

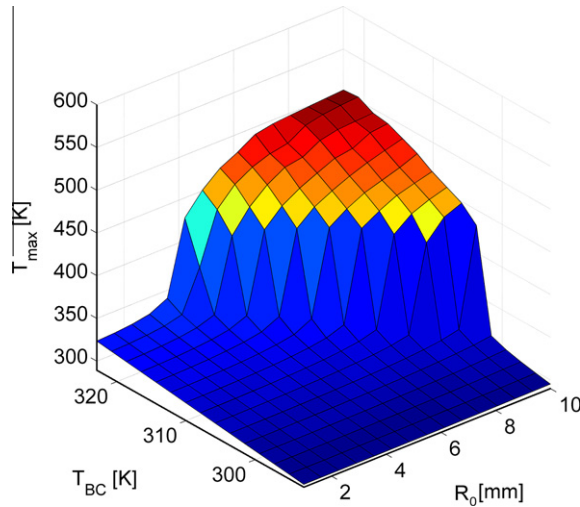
sample is again initially at room temperature. Due to the large size and small conductivity the temperature field is mainly governed by the heat generation. Heat is generated near  $r = 0$  more rapidly than it can be conducted to the boundary and the reaction is accelerating itself. Once the reaction is complete, the sample starts cooling due to the gradient between the center and the boundary. In this particular example the maximum temperature was over 400 K.

## 8. Parameter study

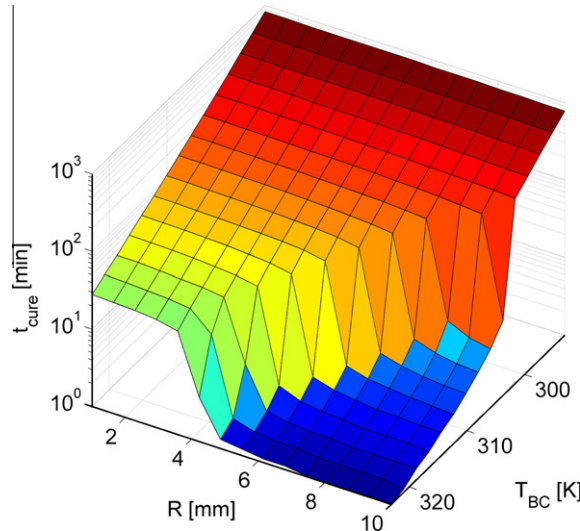
It was shown in Section 7 that a change in the radius of the cylinder can affect the spatial and time variation of the temperature and degree of cure. This suggests an investigation of the effect of the various parameters on the curing time and maximum temperature in the cylinder.

Fig. 19 shows the maximum temperature in a cylindrical specimen as a function of boundary temperature and the sample radius (the initial temperature was always set to 293 K). The maximum temperature is defined as the highest temperature at any radius or time during the process. Generally one can observe that the higher the initial temperature, the higher the maximum temperature. Also the larger the radius, the higher is the maximum temperature. It is very interesting to note that there is a transition region where the maximum temperature rapidly increases for small increases in either cylinder radius or initial/boundary temperature.

Fig. 20 shows how the curing time  $t_{cure}$  varies with sample radius and boundary temperature. Time is plotted on a logarithmic scale since a small change in temperature can cause very large changes in magnitude of the time that it takes to cure.



**Fig. 19.** Maximum temperature for different sample radii 1–10 mm and initial temperatures 293–323 K, conductivity 0.20 W/m/K.



**Fig. 20.**  $t_{cure}$  for different sample radii 1–10 mm and initial temperatures 293–323 K, Conductivity 0.20 W/m/K.

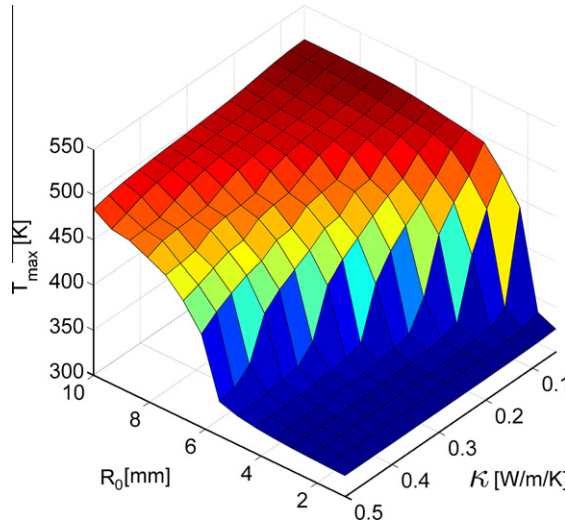


**Fig. 21.** Maximum temperature for different sample radii, 5–100 mm, and thermal conductivities 0.05–0.5 W/m/K with boundary temperature 323 K.

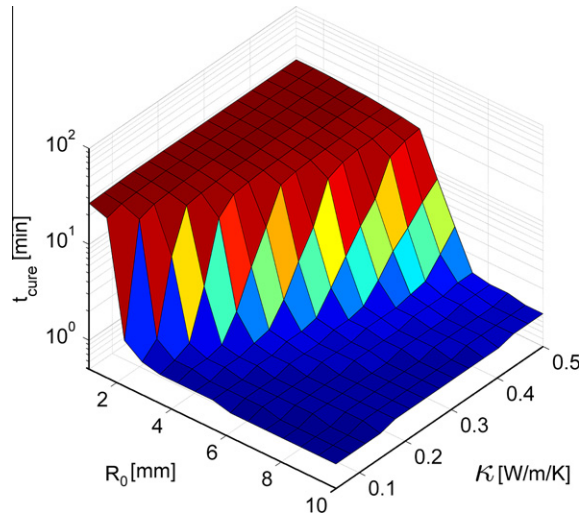


**Fig. 22.**  $t_{\text{cure}}$  for different sample radii, 5–100 mm, and thermal conductivities ranging from 0.05 to 1 W/m/K with initial temperature 303 K.

The results are closely related to the ones for the maximum temperature. The higher the temperature and the larger the radius, the faster the sample cures. The differences in time span 3 orders of magnitude. At 323 K a 4 mm diameter sample can be cured in a minute and a 1 mm sample cures in half an hour. On the other hand, at room temperature a 4 mm sample takes minutes to cure, but a 1 mm sample at room temperature takes half a day. For low temperatures and small sample sizes the degree of cure evolves as in the case of a perfect conductor. Here the heat supply due to cure is conducted quickly enough to prevent a rise in temperature. For sufficiently large boundary temperatures and sample radii the curing process resembles the one found in the perfect insulator. Here the heat supply due to cure is substantially larger than the heat that may be conducted to the boundary. As shown in Fig. 20 both regions are divided by a steep transition region where the curing time rapidly decreases for small increases in either temperature or sample radius.

Fig. 21 shows the relationship between the maximum temperature in a cylinder, the cylinder radius  $R_0$  and the thermal conductivity  $\kappa$  of the epoxy. As expected a large radius and a low conductivity causes the maximum temperature to rise.

Fig. 22 shows  $t_{\text{cure}}$  vs. radius and thermal conductivity  $\kappa$ . For low conductivity and large radii, the cure progresses rapidly.

The value of the thermal conductivity  $\kappa$  has been the subject of past research. Varshney et al. (2008) investigated the conductivity of Epon 862, curing agent W (DETDA) and their cross linked network with non-equilibrium (NEMD) and equilibrium molecular dynamics (EMD). The values obtained with NEMD were 0.21, 0.20 and 0.30 W/m/K and with EMD, they were 0.13, 0.15 and 0.13 W/m/K. Only initial uncrosslinked and final fully crosslinked networks were considered, but not intermediate stages. The authors state that they favor the higher values from the NEMD calculations to be more realistic. According

to Figs. 21 and 22, these values fall in a range where small changes in  $\kappa$  can have a large influence on maximum temperature and curing time.

## 9. Stress development

The generation of heat influences the stresses and deformations during polymer cure. To investigate stress development, a network model of a polymer will be adopted. The networks interpenetrate each other, i.e. they occupy the same volume. The assumption is made that they do not interact with each other.

A second assumption is related to the interaction of the different physical effects mentioned earlier: heat conduction, chemical change and mechanical response. Curing of epoxy resins is often done under pressure. This has influence on the rate of cure and can be taken into account. Ramos et al. (2005) measured and modeled the cure kinetics and shrinkage for a DGEBA/ MCDEA epoxy system. The reaction rate was investigated over a range of 200–600 bar pressure and a shift in reaction rate was noticeable. For this kind of analysis, where the stress and chemical composition depend on each other, the term mechanochemistry has been used in the past (Beyer & Clausen-Schaumann, 2005). Ramos et al. (2005) suggested to augment equations (5) and (6) such that:

$$k_i(T, p) = A_{i0} \exp\left(-\frac{\Delta E_i}{TR}\right) \exp\left[\left(\frac{-\Delta V}{TR} + \frac{1}{V} \frac{\partial V}{\partial p}\right)(p - p_0)\right], \quad i = 1, 2, \quad (21)$$

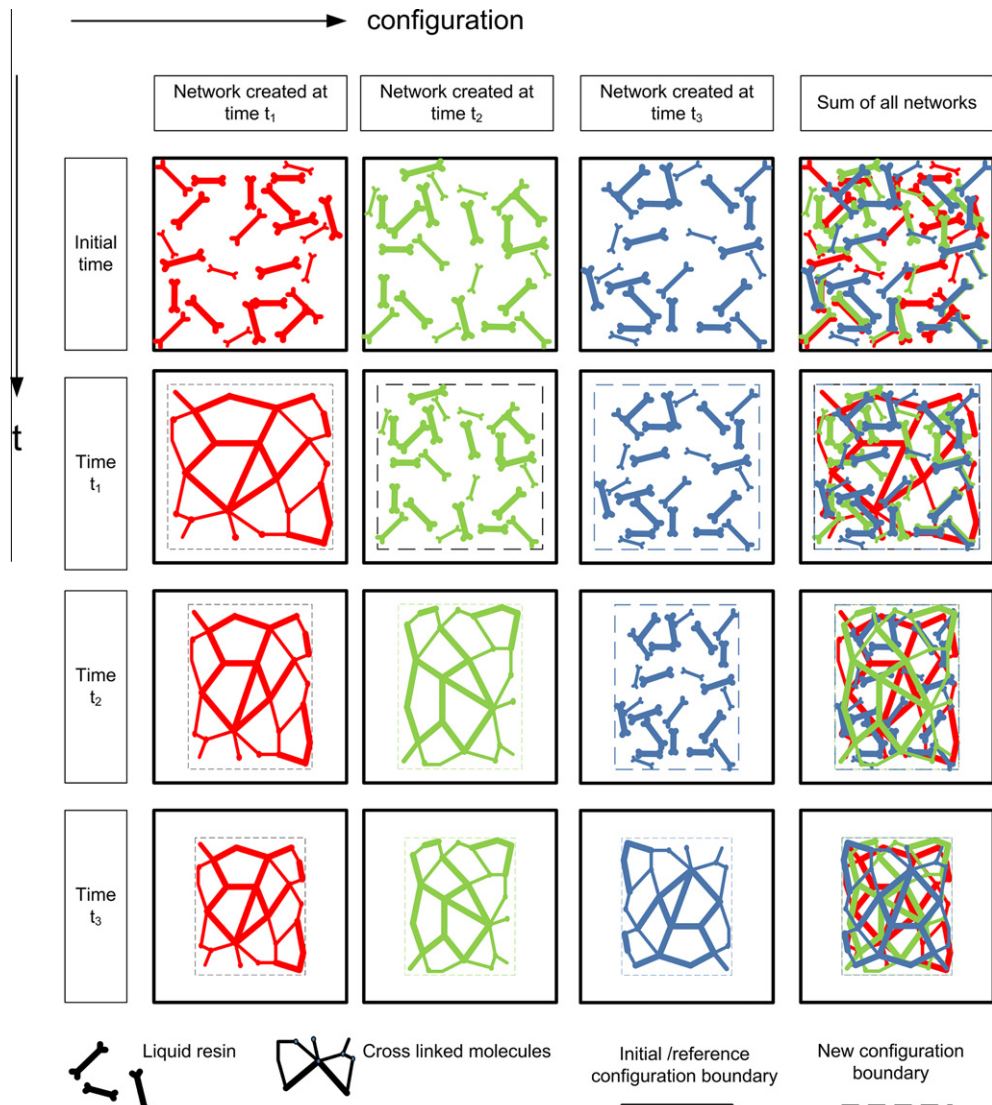
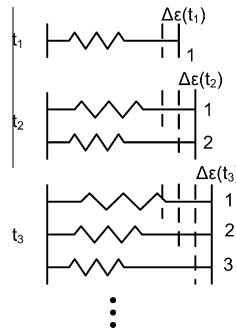


Fig. 23. A schematic of the forming of networks as curing evolves.



**Fig. 24.** Forming of 1D networks, shown schematically.

where  $\Delta V$  is the activation volume and  $p$  is the pressure. The dependency of rate of cure on temperature is significantly stronger than on pressure in the range 1–140 bar, which is observed during the curing process in the mold (Ikegawa, Hamada, & Maekawa, 1996; Revello, Saggese, & Gaiero, 2000; Rudd, 2001). Therefore, the dependency on pressure will be ignored. It is also desirable to separate the thermo-chemical problem from the mechanical problem from a numerical point of view. This leads to a one way coupling. The temperature and chemical composition are assumed to be independent of stress state but the stress state depends on the degree of cure through evolving material properties and on temperature through thermal expansion.

In what follows, a model for stress evolution that incorporates the notion of networks forming and contributing to evolving stiffness is derived for a 1D model and then generalized to three dimensions. The creation of the epoxy networks as curing evolves is depicted in Fig. 23 (Mai et al., 1998; Mei, 2000). Initially, hardener and epoxy resin are in a liquid state. They are mixed and poured into a mold, with or without fibers. Immediately after mixing, the epoxy resin starts reacting, forming cross links. At some time  $t_1$  the first network forms. It is assumed that it forms in a stress free configuration. Formation of the network is accompanied by some shrinkage due to cure. There also can be additional strain due to changes in temperature and externally applied loads. At some later time,  $t_2$ , another network forms. This network has a different stress free reference configuration. Even later, a new network forms at time  $t_3$  and this process continues in time. The stress free reference configuration for the network formed at time  $t_3$  is different than the one from the networks formed at time  $t_1$  and  $t_2$ . Because all networks occupy the same volume, their current configuration is the same. On the other hand their stress free reference configuration is different. As a result, the stress state in each network is different. The sum of all stresses within the networks is such that it balances out all externally applied resultant forces.

Fig. 24 depicts schematically the network formation process using one dimensional springs. The derivation is similar to the ones given by Mei (2000) and Hossain, Possart, and Steinmann (2009). A network forms at time  $t_1$  and experiences some external strain due to external load. The response of the network is assumed to be elastic. The stress  $\sigma(t,s)$  at time  $t$  in a network created at time  $s$  is proportional to the mechanical strain  $\epsilon^{mech}(t,s)$  relative to its stress free reference configuration multiplied by the elastic modulus  $E(s)$  associated with that network

$$\sigma(t,s) = E(s)\epsilon^{mech}(t,s). \quad (22)$$

The total strain at time  $t$  in the network formed at time  $s$ ,  $\epsilon(t,s)$ , is the sum of all incremental strains since its creation. Thus, it is the sum of the mechanical strain, thermal strain and shrinkage strain.  $\Delta\epsilon(t_i)$  is the increment in total strain from time  $t_{i-1}$  to time  $t_i$ . Therefore,

$$\epsilon(t,s) = \Delta\epsilon(s) + \Delta\epsilon(s + \Delta t) + \dots + \Delta\epsilon(s + n\Delta t) + \dots + \Delta\epsilon(t) \quad (23)$$

$$= \epsilon^{mech}(t,s) + \alpha(s)(T(t) - T(s)) - \epsilon_c(s). \quad (24)$$

Here,  $\epsilon_c(s)$  is the shrinkage strain of the network formed at time  $s$ . The sign of  $\epsilon_c(s)$  is positive when it decreases the strain. The stress in network 1 at time  $t_1$ , when it is created is,

$$\sigma(t_1, t_1) = E(t_1)(\Delta\epsilon(t_1) + \epsilon_c(t_1) - \alpha(T(t_1) - T(t_1))). \quad (25)$$

Curing strains begin to impact each network, after it is formed. Strains due to external loads and temperature differences have to be accounted for at all times. The stresses in network 1 and 2 at the formation time of network 2 are given by:

$$\sigma(t_2, t_1) = E(t_1)(\Delta\epsilon(t_1) + \Delta\epsilon(t_2) + \epsilon_c(t_1) - \alpha(T(t_2) - T(t_1))), \quad (26)$$

$$\sigma(t_2, t_2) = E(t_2)(\Delta\epsilon(t_2) + \epsilon_c(t_2) - \alpha(T(t_2) - T(t_2))). \quad (27)$$

Furthermore, in the next step, the total strains of the reference configuration change by the amount  $\Delta\epsilon_3$  after network 3 is created:

$$\sigma(t_3, t_1) = E(t_1)(\Delta\epsilon(t_1) + \Delta\epsilon(t_2) + \Delta\epsilon(t_3) + \epsilon_c(t_1) - \alpha(T(t_3) - T(t_1))), \quad (28)$$

$$\sigma(t_3, t_2) = E(t_2)(\Delta\varepsilon(t_2) + \Delta\varepsilon(t_3) + \varepsilon_c(t_2) - \alpha(T(t_3) - T(t_2))), \quad (29)$$

$$\sigma(t_3, t_3) = E(t_3)(\Delta\varepsilon(t_3) + \varepsilon_c(t_3) - \alpha(T(t_3) - T(t_3))). \quad (30)$$

Each network is weighted to contribute to the total load carrying capability in a “rule of mixtures” sense. During the creation of each network, the overall epoxy has cured by an amount  $\Delta\phi(t_i) = \phi(t_i) - \phi(t_{i-1})$ , where,  $\phi$  denotes the degree of cure as defined by Eq. (1). In the following, it will be assumed that an equivalent interpretation of the degree of cure  $\phi$  is given by

$$\begin{aligned} \phi(t) &= \frac{\text{mass cured at time } t}{\text{total mass of material that can cure}} \\ &= \text{mass fraction of cured material} \\ d\phi &= \text{mass fraction cured during the time interval from } s \text{ to } s+ds \end{aligned}$$

The total stress in the epoxy at time  $t_N$  is given by:

$$\sigma_{tot}(t_N) = \sum_{i=1}^N \Delta\phi(t_i) \sigma(t_N, t_i) = \sum_{i=1}^N \Delta\phi(t_i) E(t_i) \left( \varepsilon_c(t_i) - \alpha(T(t_N) - T(t_i)) + \sum_{j=i}^N \Delta\varepsilon(t_N, t_j) \right) \quad (31)$$

The *tot* subscript will be omitted in the following, when it is clear that the total stress is meant. When taking the limit of the above equation, the sums can be converted into integrals:

$$\sum \Delta\phi \rightarrow \int d\phi \quad \text{and} \quad \sum \Delta\varepsilon \rightarrow \int d\varepsilon$$

The discrete quantity  $\varepsilon_c(t_i)$  represents the shrinkage strain in the  $i^{th}$  network formed at time  $t_i$ . Its continuous equivalent is  $\varepsilon_c(s)$ . Equivalent expressions exist for the material properties  $E(t_N) \rightarrow E(s)$  and  $\alpha(t_N) \rightarrow \alpha(s)$ . With these substitutions, the stress up to a certain amount of cure, represented by the cure fraction,  $\Phi$  is given by:

$$\sigma(\Phi) = \int_0^\Phi \tilde{E}(\phi) \left( \varepsilon_c(\phi) - \alpha(T(\Phi) - T(\phi)) + \int_{\varepsilon(\phi)}^{\varepsilon(\Phi)} d\bar{\varepsilon} \right) d\phi \quad (32)$$

$$= \int_0^\Phi \tilde{E}(\phi) (\varepsilon_c(\phi) - \alpha(T(\Phi) - T(\phi)) + \varepsilon(\Phi) - \varepsilon(\phi)) d\phi. \quad (33)$$

The degree of cure  $\phi(s)$  increases monotonically with time which allows for the substitution,  $d\phi = \frac{d\phi}{ds} ds$ :

$$\sigma(t) = \int_0^t \frac{d\phi}{ds} E(s) (\varepsilon(t) - \varepsilon(s) + \varepsilon_c(s) - \alpha(T(t) - T(s))) ds \quad (34)$$

The elastic modulus  $E(s)$  depends directly on the degree of cure, and indirectly on time, by  $E(s) = \tilde{E}(\phi(s))$ . The above equation can be generalized to three dimensions:

$$\begin{aligned} \underline{\underline{\sigma}} &\equiv \int_0^t \frac{d\phi}{ds} \underline{\underline{1}} \left[ K(s) \text{tr}(\underline{\underline{\varepsilon}}(t) - \underline{\underline{\varepsilon}}(s) + \underline{\underline{\varepsilon}}_c(s) - \frac{1}{2}\alpha(s)\Delta T(t, s)) + 2\mu(s) \left( \underline{\underline{\varepsilon}}(t) - \underline{\underline{\varepsilon}}(s) + \underline{\underline{\varepsilon}}_c(s) - \frac{1}{3}\text{tr}(\underline{\underline{\varepsilon}}(t) - \underline{\underline{\varepsilon}}(s) + \underline{\underline{\varepsilon}}_c(s)) \right) \right] \\ &\quad + (1 - \phi(t)) K_{liq} \text{tr}(\underline{\underline{\varepsilon}}(t) - \frac{1}{2}\alpha_{liq}\Delta T(t)) \underline{\underline{1}} \end{aligned} \quad (35)$$

where  $K$  is the per-network bulk modulus,  $\mu$  is the per-network shear modulus and  $\alpha$  is the linear coefficient of thermal expansion of each network.  $K_{liq}$  and  $\alpha_{liq}$  are the bulk modulus and coefficient of thermal expansion of the uncured liquid epoxy resin. The notation,  $(\underline{\underline{\cdot}})$  indicates a second order tensor. The last term represents the contribution to the total stress from the volume fraction of uncured epoxy liquid. The liquid can hold compressive stress but its shear stress is neglected.

The tensor quantity  $\underline{\underline{\varepsilon}}_c(s)$  describes the cure shrinkage strains of each network. It is assumed that curing only produces equal normal strains

$$\underline{\underline{\varepsilon}}_c(s) = \begin{bmatrix} \varepsilon_c(s) & 0 & 0 \\ 0 & \varepsilon_c(s) & 0 \\ 0 & 0 & \varepsilon_c(s) \end{bmatrix} \quad (36)$$

$\underline{\underline{\varepsilon}}_c(s)$  can be chosen such that macroscopically, shrinkage as a linear function of degree of cure can be observed.

It is noted that formally  $\alpha(s)$ ,  $\mu(s)$ ,  $K(s)$  are functions of time. But actually they are a function of cure, which has to be related to time, so that  $\alpha(s) = \tilde{\alpha}(\phi(s))$ ,  $\mu(s) = \tilde{\mu}(\phi(s))$ ,  $K(s) = \tilde{K}(\phi(s))$  and  $\varepsilon_c(s) = \tilde{\varepsilon}_c(\phi(s))$ . These material functions are determined from experiments. There is a small dependence of absolute final degree of cure on the curing temperature in (35). In average the final degree of cure increases with increasing curing temperature. However, the experimental scatter within each curing level is larger than the deviation of the final absolute degree of cure. Therefore the final degree of cure is assumed to be independent of temperature.

## 10. Mechanical material properties

### 10.1. Elastic properties

The longitudinal modulus, shear modulus and degree of cure are measured as a function of time through concurrent Raman (RLS) and Brillouin (BLS) light scattering (Chike et al., 1993; Merad et al., 2009; Philipp et al., 2011; Sanctuary et al., 2010; Sui, Huang, Podsiadlo, Kotov, & Kieffer, 2010; Yamura, Matsukawa, Otani, & Ohtori, 1999). The longitudinal modulus  $M$  is the elastic constant measured in a uniaxial strain field. It is related to the Lamé constants and the bulk modulus by  $M = \lambda + 2\mu = K + \frac{4}{3}\mu$ . Raman scattering provides cure information and Brillouin light scattering provides mechanical information. Furthermore, the measurements are carried out concurrently, i.e., the signals for both measurements were collected at the same time from the same focal volume of the probing laser beam. These optical measurement methods have the advantage of yielding mechanical and chemical properties non-destructively and without perturbing the thermodynamic equilibrium of the probed system. In contrast, classical methods that measure the mechanical properties during cure, such as rheometers or bending tests (O'Brian, Mather, & White, 2001), actively influence the boundary value problem that is needed to extract the per-network properties for this approach.

It is important to note that experimentally, the response of all networks is measured simultaneously. The individual response of each network has to be adjusted so that the total simulated response follows the total experimentally measured response. To this end, assume that the network is cured in a uniaxial strain field. After some time, a sudden jump in strain is applied. The jump needs to be considered for all times during the curing history, because the material properties need to be extracted for all times during the curing history. The stress response is measured in the direction the strain jump is applied, and in the perpendicular direction. The boundary value problem (BVP) is depicted in Fig. 25.

The strain tensor of the uniaxial strain field, corresponding to before and after a small increment in strain, are:

$$\underline{\underline{\varepsilon}} = \begin{bmatrix} \varepsilon & 0 & 0 \\ 0 & 0 & 0 \\ 0 & 0 & 0 \end{bmatrix} \quad (37)$$

and,

$$\underline{\underline{\varepsilon}} = \begin{bmatrix} \varepsilon + \Delta\varepsilon & 0 & 0 \\ 0 & 0 & 0 \\ 0 & 0 & 0 \end{bmatrix}, \quad (38)$$

respectively. Ignoring the influence of temperature, the stresses before and after the jump, respectively, are:

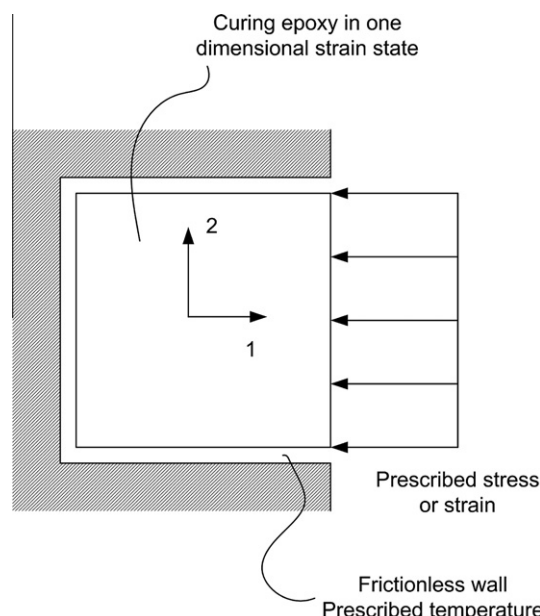


**Fig. 25.** Uniaxial strain boundary value problem used to determine material properties.

$$\underline{\underline{\sigma}} = \begin{bmatrix} \sigma_{11} & 0 & 0 \\ 0 & \sigma_{22} & 0 \\ 0 & 0 & \sigma_{33} = \sigma_{22} \end{bmatrix} \quad (39)$$

$$\underline{\underline{\sigma}} + \Delta\underline{\underline{\sigma}} = \begin{bmatrix} \sigma_{11} + \Delta\sigma_{11} & 0 & 0 \\ 0 & \sigma_{22} + \Delta\sigma_{22} & 0 \\ 0 & 0 & \sigma_{33} = \sigma_{22} + \Delta\sigma_{22} \end{bmatrix}. \quad (40)$$

Thus,

$$\sigma_{11} = \int_0^t \dot{\phi} \left\{ K[\varepsilon(t) - \varepsilon(s) + 3\varepsilon_c(s)] + \frac{4}{3}\mu[\varepsilon(t) - \varepsilon(s)] \right\} ds + (1 - \phi(t))K_{liq}\varepsilon(t), \quad (41)$$

$$\sigma_{11} + \Delta\sigma_{11} = \int_0^t \dot{\phi} \left\{ K[\varepsilon(t) + \Delta\varepsilon - \varepsilon(s) + 3\varepsilon_c(s)] + \frac{4}{3}\mu[\varepsilon(t) + \Delta\varepsilon - \varepsilon(s)] \right\} ds + (1 - \phi(t))K_{liq}(\varepsilon(t) + \Delta\varepsilon). \quad (42)$$

The difference between the two is

$$\Delta\sigma_{11} = \Delta\varepsilon \int_0^t \dot{\phi} \left\{ K(s) + \frac{4}{3}\mu(s) \right\} ds + \Delta\varepsilon(1 - \phi)K_{liq}, \quad (43)$$

$$= \Delta\varepsilon \int_0^t \dot{\phi}M(s)ds + \Delta\varepsilon(1 - \phi)K_{liq}. \quad (44)$$

Thus, the incremental stress-strain relations can be written as,

$$\Delta\sigma_{11} = \Delta\varepsilon_{11}M_{tot}(t), \quad (45)$$

where

$$M_{tot} = \int_0^t \dot{\phi}M(s)ds + (1 - \phi(t))K_{liq} \quad (46)$$

$$= \int_0^t \dot{\phi} \left\{ K(s) + \frac{4}{3}\mu(s) \right\} ds + (1 - \phi(t))K_{liq} \quad (47)$$

is the total longitudinal modulus, and  $M(s)$  is the longitudinal modulus of each network formed at time  $s$ . Differentiating with respect to time,  $t$ , re-arranging and applying the chain rule yields the per-network properties

$$M(\phi) = \frac{dM_{tot}(\phi)}{d\phi} + K_{liq}. \quad (48)$$

The same BVP can be used to determine a second set of properties. For the direction perpendicular to the one in which the strain is applied, it follows that:

$$\Delta\sigma_{22} = \Delta\varepsilon \int_0^t \dot{\phi}(K(s) - \frac{2}{3}\mu(s))ds + \Delta\varepsilon(1 - \phi)K_{liq} \quad (49)$$

$$= \Delta\varepsilon \int_0^t \dot{\phi}\lambda(s)ds + \Delta\varepsilon(1 - \phi)K_{liq}. \quad (50)$$

For this particular BVP,

$$\Delta\sigma_{22} = \Delta\varepsilon_{11}\lambda_{tot}(t), \quad (51)$$

where

$$\lambda_{tot} = \int_0^t \dot{\phi}(s)\lambda(s)ds + (1 - \phi(t))K_{liq} \quad (52)$$

so that the per-network Lamé constant is

$$\lambda(\phi) = \frac{d\lambda_{tot}(\phi)}{d\phi} + K_{liq}. \quad (53)$$

This can be transformed to yield the per network shear and bulk moduli:

$$\mu(\phi) = \frac{d\mu_{tot}}{d\phi}, \quad (54)$$

$$K(\phi) = \frac{dK_{tot}}{d\phi} + K_{liq}. \quad (55)$$

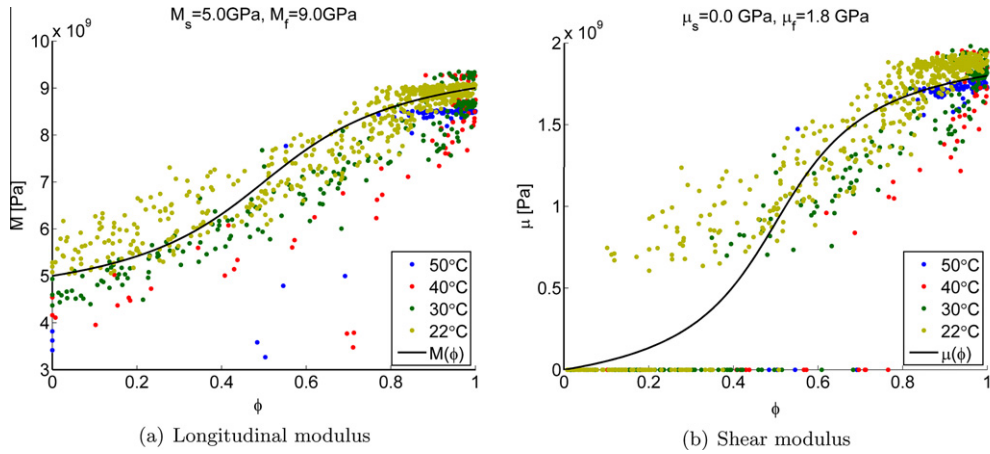


**Fig. 26.** Experimental results and curve fit of Brillouin and Raman light scattering.

Fig. 26(a) and (b) shows representative experimental data for  $M$  and  $\mu$  as functions of extent of cure. For mathematical convenience the transition of these material properties is currently modeled with an analytical function:

$$\mu_{\text{tot}}(\phi) = \frac{\arctan\left((\phi - \frac{1}{2})\beta_\mu\right)}{\arctan\left(\frac{\beta_\mu}{2}\right)} (\mu_f - \mu_s) + \left(\frac{\mu_f + \mu_s}{2}\right), \quad (56)$$

$$M_{\text{tot}}(\phi) = \frac{\arctan\left((\phi - \frac{1}{2})\beta_M\right)}{\arctan\left(\frac{\beta_M}{2}\right)} (M_f - M_s) + \left(\frac{M_f + M_s}{2}\right), \quad (57)$$

$\mu_s$ ,  $\mu_f$ ,  $M_s$ ,  $M_f$  are the start and final value of the measure shear modulus and longitudinal modulus, respectively.  $\beta_\mu$  and  $\beta_M$  are fitting constants of the experimental data, related to the curvature of the experimental fit. This leads to closed form solutions for the per-network properties:

$$\mu(\phi) = \frac{1}{2} \frac{\beta_\mu(\mu_f - \mu_s)}{\left(1 + (\phi - 1/2)^2 \beta_\mu^2\right) \arctan(1/2\beta_\mu)}, \quad (58)$$

$$M(\phi) = \frac{1}{2} \frac{\beta_M(M_f - M_s)}{\left(1 + (\phi - 1/2)^2 \beta_M^2\right) \arctan(1/2\beta_M)} + K_{liq}, \quad (59)$$

$$K(\phi) = M(\phi) - \frac{4}{3} \mu(\phi). \quad (60)$$

In the presented curing model, a small amount of shear stiffness is assumed even for low degrees of cure, as shown in Fig. 26(b). This is necessary for two reasons: as can be seen from Eq. (54) a discontinuity in the total shear modulus would lead to a singularity of the per-network shear modulus in the context of the proposed curing model. Secondly, the finite element procedure uses solid elements that require a non-zero shear stiffness. On the other hand, it should be noted that in reality the epoxy behaves like a viscous liquid until gelation occurs. Only from that moment onward a finite shear modulus is detected. During the simulations it was found that despite the assumption of a small amount of shear modulus for a low degree of cure no appreciable stress level was detected during the early phase of the curing process.

Finally, the bulk modulus of the liquid epoxy is the one measured at the beginning of the experiment

$$K_{liq} = K_{\text{tot}}(0) = M_{\text{tot}}(0). \quad (61)$$

## 10.2. Cure shrinkage

To determine the correct cure shrinkage a boundary value problem needs to be formulated, where the change in volume can be measured. Therefore, consider again the uniaxial strain BVP of a curing epoxy sample as shown in Fig. 25. The specimen is free to expand or contract in the 1-direction. No stresses are applied in this direction. The stress and strain tensors are,

$$\underline{\sigma} = \begin{bmatrix} \sigma_{11} = 0 & 0 & 0 \\ 0 & \sigma_{22} & 0 \\ 0 & 0 & \sigma_{33} = \sigma_{22} \end{bmatrix} \quad (62)$$

**Table 3**

Cure shrinkage in various epoxy materials.

Cure shrinkage/volume change	Material	Reference
6.9%	MY750	Li et al. (2004)
4.5@100°C, 200 bar	DGEBA/MCDEA	Ramos et al. (2005)
>1%	Epon 828/DEA	Adolf and Chambers (1997)
2.75% after gelation	Bisphenol F	Lange et al. (1997)
<2%	Epikote 828/MNA/BDMA	Yates et al. (1979)
2%	Current study	

and

$$\underline{\varepsilon} = \begin{bmatrix} \varepsilon & 0 & 0 \\ 0 & 0 & 0 \\ 0 & 0 & 0 \end{bmatrix}. \quad (63)$$

The stress in the 1-direction is given by

$$\sigma_{11} = \int_0^t \dot{\phi}(s) M(s)(\varepsilon(t) - \varepsilon(s)) ds + 3 \int_0^t \varepsilon_c(s) K(s) \dot{\phi}(s) ds + (1 - \phi(t)) \varepsilon(t) K_{liq} \quad (64)$$

and it is equal to zero. There is a monotonic relation between time,  $t$ , and degree of cure,  $\phi$ . A change in variables of  $t \rightarrow \Phi = \phi(t)$  and  $\dot{\phi} ds \rightarrow d\phi$  leads to:

$$\sigma_{11}(\Phi) = \int_0^\Phi M(\phi)(\varepsilon(\Phi) - \varepsilon(\phi)) d\phi + 3 \int_0^\Phi \varepsilon_c(\phi) K(\phi) d\phi + (1 - \Phi) \varepsilon(\Phi) K_{liq} = 0. \quad (65)$$

Differentiating with respect to the upper limit, observing that no stress was applied in the 1-direction and rearranging, yields the final expression for the cure shrinkage in terms of the strain in the direction of the free surface;

$$\varepsilon_c(\Phi) = \frac{1}{3K(\Phi)} \left[ \left( \varepsilon(\Phi) - (1 - \Phi) \frac{d\varepsilon(\Phi)}{d\Phi} \right) K_{liq} - \frac{d\varepsilon(\Phi)}{d\Phi} \int_0^\Phi M(\phi) d\phi \right]. \quad (66)$$

The total cure shrinkage of all networks  $\varepsilon(\Phi)$  can be measured through a gravimetric test method (Li, Potter, Wisnom, & Stringer, 2004). Table 3 gives an account of the results that have been obtained for various epoxy systems.

## 11. Curing of pure epoxy

The generation of stresses due to thermal and curing gradients will be illustrated using the example of pure epoxy blocks. The temperature, degree of cure and cure stress development in a pure epoxy cube will be considered. Two different size cubes are considered in order to show the effect of size on curing. The generic cube is shown in Fig. 27. The cubes have side length of 1 mm and 8 mm, respectively. Due to the symmetric nature of the boundary value problem, the size of the finite element model can be reduced to 1/8th. The boundary conditions on the original cube are such that the outside surfaces are traction free. The temperature on the entire boundary is prescribed. The epoxy is completely uncured at 295 K (22 °C) at time  $t = 0$ . The temperature is ramped up linearly within 100 s to 323 K (50 °C). It is held at that level subsequently for 3600 s. The boundary temperature is then reduced to room temperature within 100 s. This boundary temperature time history is shown

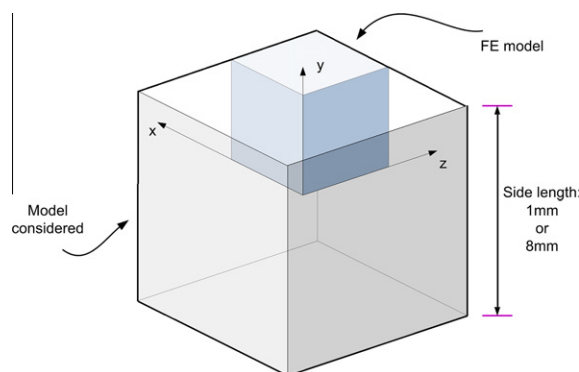


Fig. 27. Pure epoxy cube, symmetry has been used, to reduce model size to one eights.

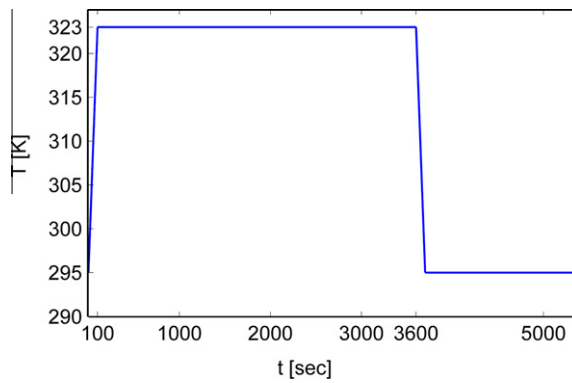


Fig. 28. Temperature history used for thermal boundary conditions.

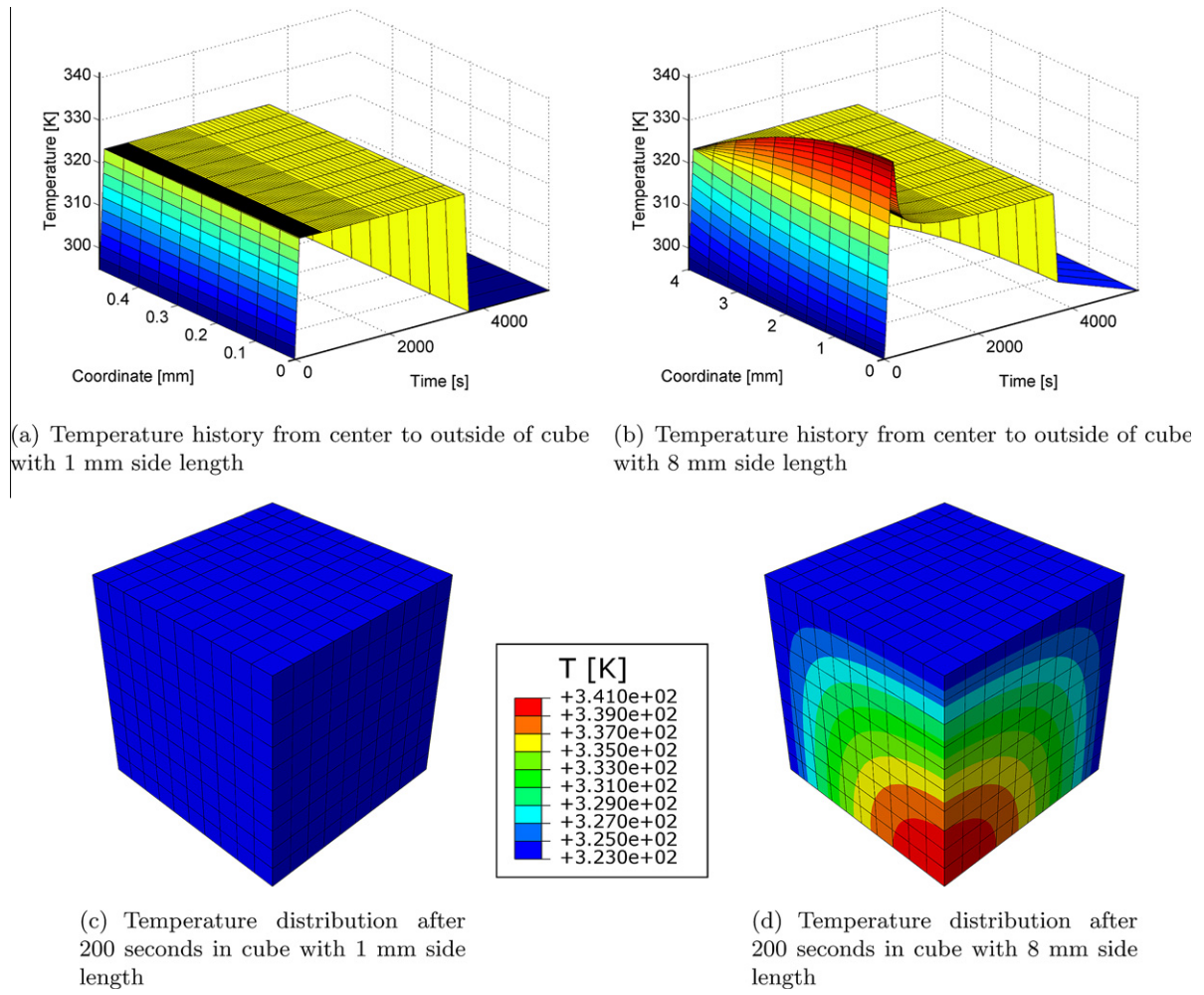
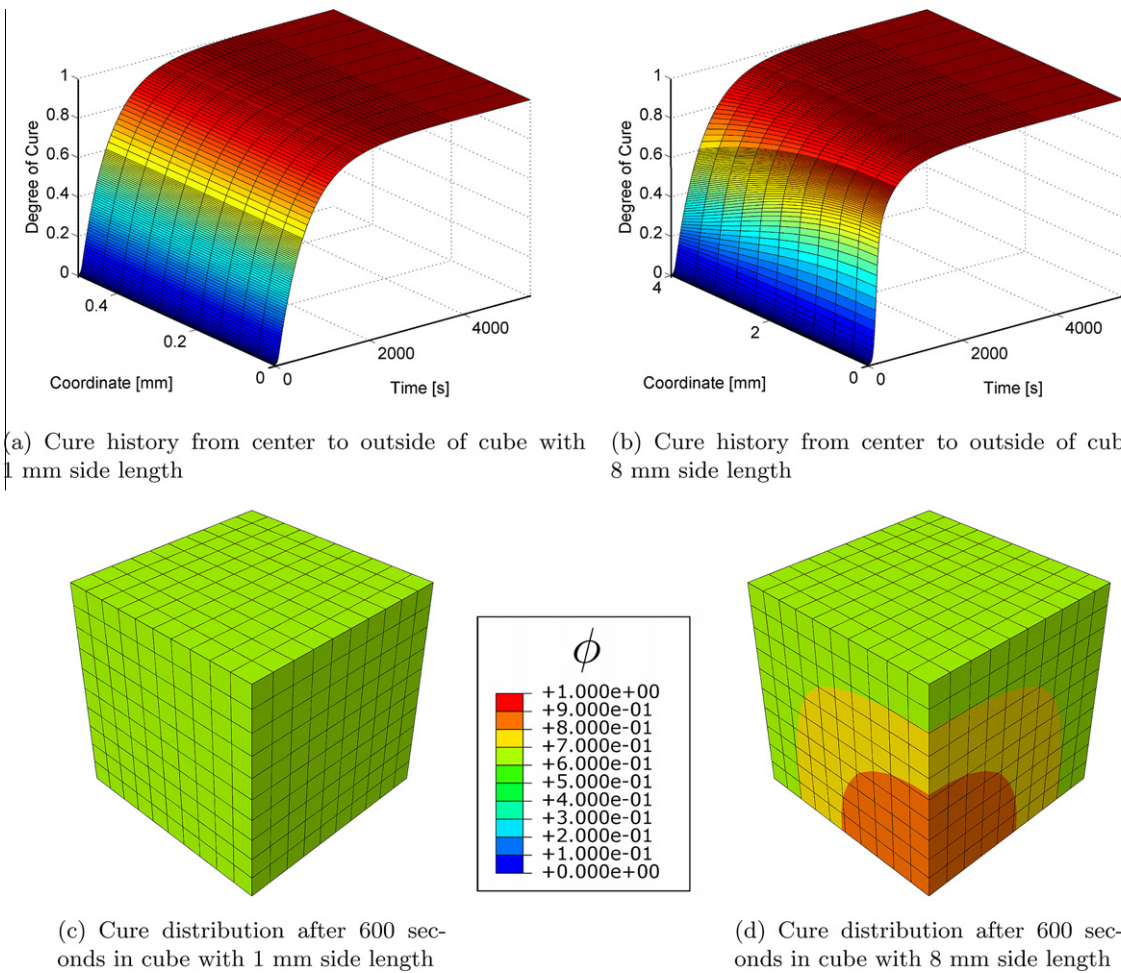


Fig. 29. Temperature history in small and large block of epoxy.

in Fig. 28. In the symmetric FE model, the boundary conditions on the outside are identical to the original model. The origin of the coordinate system is at a corner on an inner surface. On the inner “cut planes” symmetry demands that the normal displacements are set to zero. Also, the heat flux is zero on these planes, which is equivalent to a perfectly insulating wall.

Fig. 29 shows the temperature fields in the two cubes as they cure. As can be seen in Fig. 29(a), the temperature is uniform in the small sample throughout the entire time and follows the prescribed boundary condition very closely. On the other



**Fig. 30.** Cure history in small and large block of epoxy.

hand, in the larger sample the temperature is not uniform. During the time at which the boundary temperature is ramped up, the inside temperature lags the outside temperature. That means that during the first 100 s, the slope of the degree of cure is lower in the center compared to the outside. The low conductivity of the material puts a limit on how quickly a steady or uniform state is reached. Due to the exothermic reaction of the epoxy, heat or energy will be released into the system. This heat causes the temperature to rise in the large sample. Low conductivity limits the size of the heat flux and excess heat cannot be transported to the boundary quickly enough to reach a uniform distribution. The result is an overshoot in temperature, which itself leads to even quicker cure. Once the curing rate decreases, the heat released into the system diminishes and a uniform distribution is reached eventually. Finally, upon cooling of the sample the center lags again behind the boundary. In this particular case, the center remains at an elevated temperature for a longer time. It should be noted, that upon change of boundary conditions of the small sample, the temperature there is also not uniform. This would occur only for the case for a perfect conductor, but in the actual simulation, temperature gradients are too small to be noticed and properly resolved.

Fig. 30 shows the curing history of the small and large epoxy samples. Since temperature and cure are closely related, it is not surprising that the uniform temperature distribution in the small sample gives rise to a uniform degree of cure distribution. In the large sample, however, initially the rate of cure is slower at the center compared to the outside. That means that the slope indicating the rate of cure is lower during the first 100 s. This is true until the inside temperature reaches the same level as the outside. As mentioned before, since heat emitted to the system cannot be transported to the outside quickly enough, the temperature rises at the center of the specimen. This in turn leads to faster cure and more heat released into the system in a shorter time. Therefore full cure is attained faster on the inside. It should be noted that Fig. 29(d) shows the temperature distribution 200 s after the reaction started. At this point the temperature gradient is largest in the specimen. However, Fig. 30(d) shows the time at which the difference in degree of cure is very uneven. This is at 600 s. Therefore, an overshoot in temperature should not be mistaken for a large degree of cure obtained. High degree of cure will lag behind

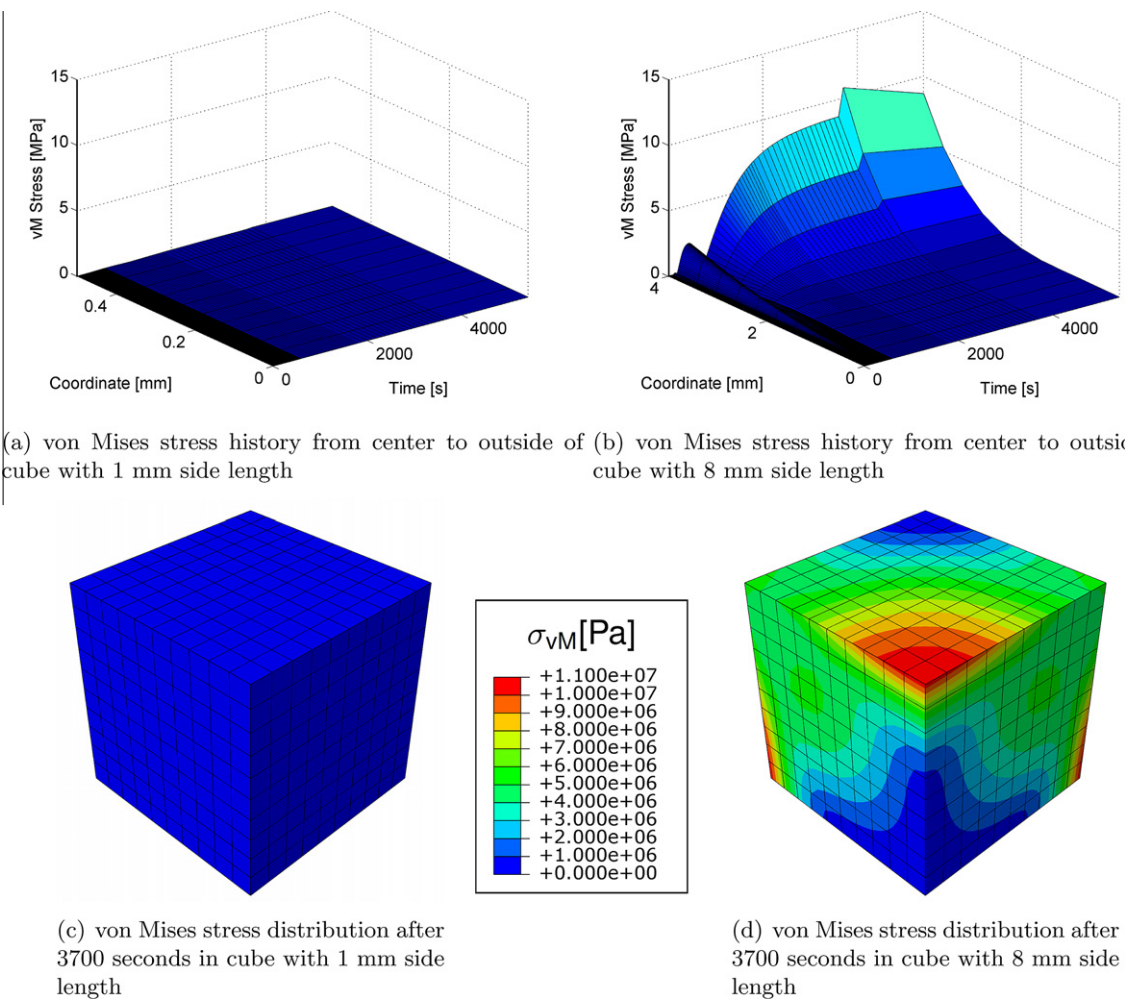


**Fig. 31.** von Mises stress history in small and large block of epoxy.

that overshoot. The reason for this behavior lies in the fact that heat released into the system is related to the rate of cure, not the degree of cure. For the Kamal model (Kamal, 1974), the rate of cure is typically higher for low degrees of cure, and reduces with increasing degree of cure.

Fig. 31 depicts the von Mises stresses in the small and large epoxy samples. The von Mises stress is a common scalar field to quantify the stress state, and is defined as

$$\sigma_{vM}(t, s) = \sqrt{\frac{(\sigma_{xx} - \sigma_{yy})^2 + (\sigma_{yy} - \sigma_{zz})^2 + (\sigma_{zz} - \sigma_{xx})^2 + 6(\sigma_{xy}^2 + \sigma_{xz}^2 + \sigma_{yz}^2)}{2}}. \quad (67)$$

The small sample is stress free. This is expected because no thermal gradients or gradients in degree of cure are present and the sample boundary was traction free. However, the larger sample does exhibit stresses due to the *non uniform nature of the temperature and cure*. Von Mises stresses are larger on the outside than on the inside. Fig. 32 gives closer insight into what is happening. Here the maximum principal stress is shown. During the cure of the large sample the center cures first and the outside follows later. Therefore the center solidifies first. The phase transition from liquid to solid is associated with some degree of shrinkage. However this has little effect on the outer region. Its small degree of cure implies that the epoxy has a very low shear modulus,  $\mu$ , and will follow any shape change without creating significant stresses. When the outer parts of the cube cure, the center is already solidified. The cure shrinkage will therefore affect the epoxy. A decrease of volume upon phase change from liquid to solid implies that the outer part is “shrink wrapped” around the inner part. The result is the development of tensile stresses in the outer part and compressive stresses on the inside. A traction free boundary implies that the maximum tensile stresses act on a surface perpendicular to the outside surface. Therefore, if a crack or void were to be present in the material, it would have a tendency to open up further. Also, due to the symmetric nature of the boundary value problem, a near hydrostatic stress state can be assumed towards the center of the specimen. This leads

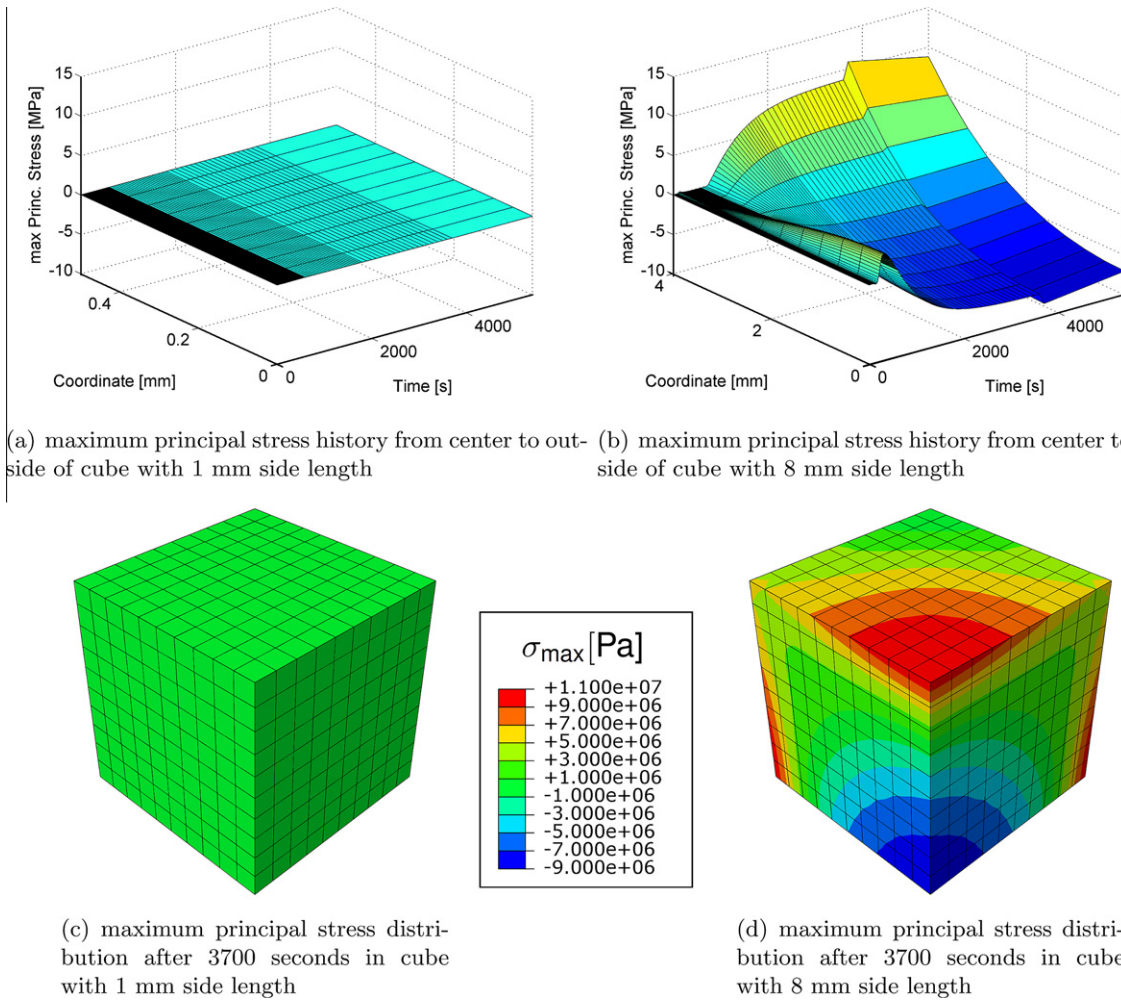


**Fig. 32.** Maximum principal stress history in small and large block of epoxy.

to vanishing von Mises stresses at the center. Finally, it should be noted that the von Mises stresses and the maximum principal stresses show a jump in Fig. 31 at 3600 s when the sample is cooled down. This is again due to the low thermal conductivity and the temperature gradient. The outside has a lower temperature than the inside. The positive coefficient of thermal expansion of the epoxy implies that the outside contracts more than the inside, amplifying the tensile stresses on the boundary and the compressive stresses in the center.

## 12. Conclusions

Several models for cure of epoxy polymers were presented and coupled with the equation for heat generation and conduction. Subsequently a model for stress generation during cure was introduced and applied to the cure of an Epon 862/Epicure 9553 specimen. Closed form solutions for temperature and chemical evolution were presented for the cases corresponding to that of a perfect conductor and a perfect insulator. It was found that the curing time between these two extremes changes by more than a factor of ten. A change in initial temperature (perfect insulator) or boundary temperature (perfect conductor) causes an exponential decrease in curing time, spanning more than two magnitudes over a range of 100 K. These results were applied to available epoxy systems. It was shown that there is a close relation between geometry, thermal conductivity, temperature and time to cure. High initial temperature, low thermal conductivity and a large size (geometry) cause high curing rates and low curing times. In these cases the curing characteristics were similar to one of a perfect insulator with a steep rise of curing rate towards full cure. For smaller sizes, higher conductivity and lower temperatures, the opposite trend was observed. The curing rate declined smoothly for higher degrees of cure. The behavior was very similar to the case of a perfect conductor. These two extremes are very useful in estimating the curing characteristics of components with different size scales. Maximum temperature during cure ( $T_{max}$ ), and curing time ( $t_{cure}$ ), can be used

as two critical parameters to characterize the curing process. There is only a small transition band in the size vs. initial temperature “space”, where none of these extremes apply.

To quantify the influence of temperature and curing gradients on resulting curing stresses, a network forming model is introduced. Here, the idea of continuously developing networks has been used. These networks interpenetrate each other, but do not otherwise interact with each other. Different networks may have different thermal and elastic properties and states. Especially, different networks have different stress free reference configurations. Due to thermal gradients in time and space and cure shrinkage of newly generated networks, stresses develop. The curing model was applied to a small and large epoxy cube. It was shown that the heat generation of the exothermic curing reaction combined with poor heat conduction leads to significant gradients in the temperature and degree of cure. This results in residual stresses at the end of cure in an otherwise completely homogeneous material, whose *magnitude depends on the cured volume of material*. Knowledge of these built in curing stresses, as a function of cure process and volume of material (size) is important in improving polymer based manufacturing processes, as they may reduce the margin of external loads that may be applied, before a manufactured structural part fails.

## Disclaimer

This report was prepared as an account of work sponsored by an agency of the United States Government. Neither the United States Government nor any agency thereof, nor any of their employees, makes any warranty, express or implied, or assumes any legal liability or responsibility for the accuracy, completeness, or usefulness of any information, apparatus, product, or process disclosed, or represents that its use would not infringe privately owned rights. Reference herein to any specific commercial product, process, or service by trade name, trademark, manufacturer, or otherwise does not necessarily constitute or imply its endorsement, recommendation, or favoring by the United States Government or any agency thereof. The views and opinions of authors expressed herein do not necessarily state or reflect those of the United States Government or any agency thereof.

## Acknowledgements

The authors would like to acknowledge the support of the Automotive Composites Consortium (ACC) and its Predictive/Virtual Technology Development and Crash Energy Management Group (ACC100). This material is based upon work supported by the Department of Energy under Award Number DE-FC26-02OR22910. The authors are also grateful for the financial support of the Department of Aerospace Engineering, University of Michigan.

## References

- Abhilash, P., Kannan, K., & Varkey, B. (2010). Simulation of curing of a slab of rubber, Science and technologies of specialty advanced materials and polymers for aerospace and defense and applications: the proceedings of SAMPADA-2008 conference . *Materials Science and Engineering: B*, 168(1–3), 237–241.
- Adolf, D., & Chambers, R. (1997). Verification of the capability for quantitative stress prediction during epoxy cure. *Polymer*, 38, 5481–5490.
- Adolf, D. B., & Chambers, R. S. (2007). A thermodynamically consistent, nonlinear viscoelastic approach for modeling thermosets during cure. *Journal of Rheology*, 51(1), 23–50.
- Adolf, D. B., Chambers, R. S., & Caruthers, J. M. (2004). Extensive validation of a thermodynamically consistent, nonlinear viscoelastic model for glassy polymers. *Polymer*, 45(13), 4599–4621.
- Adolf, D. B., Martin, J. E., Chambers, R. S., Burchett, S. N., & Guess, T. R. (1998). Stresses during thermoset cure. *Journal of Materials Research*, 13, 530–550.
- Beyer, M. K., & Clausen-Schaumann, H. (2005). Mechanochemistry: The mechanical activation of covalent bonds. *Chemical Reviews*, 105, 2921–2948.
- Bogetti, T. A., & Gillespie, J. W. (1992). Process-induced stress and deformation in thick-section thermoset composite laminates. *Journal of Composite Materials*, 26(5), 626–660.
- Bujard, P., Kuhlein, G., Ino, S., & Shiobara, T. (1994). Thermal conductivity of molding compounds for plastic packaging. in Proceedings of the 44th Electronic Components and Technology Conference, May 1994 (pp. 159–163).
- Chekanov, Y. A., Korotkov, V. N., Rozenberg, B. A., Dzhavadyan, E. A., & Bogdanov, L. M. (1995). Cure shrinkage defects in epoxy resins. *Polymer*, 36(10), 2013–2017.
- Chike, K. E., Myrick, M. L., Lyon, R. E., & Angel, S. M. (1993). Raman and near-infrared studies of an epoxy resin. *Applied Spectroscopy*, 47(10), 1631–1635.
- Corden, T. J., Jones, I. A., Jones, D. T., & Middleton, V. (1998). The mechanisms of interlaminar cracking in thick resin transfer moulded composite cylinders. *Composites Part A: Applied Science and Manufacturing*, 29(4), 455–464.
- Doghri, I. (2000). *Mechanics of deformable solids*. Berlin: Springer Verlag.
- Fung, Y. (1994). *A first course in continuum mechanics* (third ed.). Englewood Cliffs: Prentice Hall.
- Ganguli, S., Roy, A. K., & Anderson, D. P. (2008). Improved thermal conductivity for chemically functionalized exfoliated graphite/epoxy composites. *Carbon*, 46(5), 806–817.
- Garnier, B., & Sommier, A. (2002). Thermal property measurements during curing of thermoset resins using steady periodic conditions. *Journal of Reinforced Plastics and Composites*, 21(13), 1193–1203.
- Hexion Specialty Chemicals, Inc. Diglycidyl Ether of Bisphenol F (DGEBF) – Performance properties.
- Hossain, M., Possart, G., & Steinmann, P. (2009). A small-strain model to simulate the curing of thermosets. *Computational Mechanics*, 43, 769–779.
- Ikegawa, N., Hamada, H., & Maekawa, Z. (1996). Effect of compression process on void behavior in structural resin transfer molding. *Polymer Engineering & Science*, 36(7), 953–962.
- Kamal, M. R. (1974). Thermoset characterization for moldability analysis. *Polymer Engineering and Science*, 14(3), 231–239.
- Kannan, K., & Rajagopal, K. (2011). A thermodynamical framework for chemically reacting systems. *Zeitschrift für Angewandte Mathematik und Physik (ZAMP)*, 62, 331–363. doi:10.1007/s00033-010-0104-1.
- Lange, J., Toll, S., Månsen, J.-A. E., & Hult, A. (1997). Residual stress build-up in thermoset films cured below their ultimate glass transition temperature. *Polymer*, 38(4), 809–815.
- Lange, J., Toll, S., Månsen, J.-A. E., & Hult, A. (1995). Residual stress build-up in thermoset films cured above their ultimate glass transition temperature. *Polymer*, 36(16), 3135–3141.

- Lee, E. H., Rogers, T. G., & Woo, T. C. (1965). Residual stresses in a glass plate cooled symmetrically from both surfaces. *Journal of the American Ceramic Society*, 48(9), 480–487.
- Li, C., Potter, K., Wisnom, M. R., & Stringer, G. (2004). In-situ measurement of chemical shrinkage of my750 epoxy resin by a novel gravimetric method. *Composites Science and Technology*, 64(1), 55–64.
- Li, M., Zhu, Q., Geubelle, P. H., & Tucker, C. L. III, (2001). Optimal curing for thermoset matrix composites: Thermochemical considerations. *Polymer Composites*, 22(1), 118–131.
- Mai, Y., Yee, A. F., Wineman, A. S., & Xiao, C. (1998). Stress evolution during thermoset cure. In *Material research society symposia proceedings* (p. 515).
- Mathworks, T. (2009). Matlab R2009a.
- Mei, Y. (2000). Stress evolution in a conductive adhesive during curing and cooling. Ph.D. Thesis. Ann Arbor, Michigan: University of Michigan.
- Merad, L., Cochez, M., Margueron, S., Jauchem, F., Ferriol, M., Benyoucef, B., et al (2009). In-situ monitoring of the curing of epoxy resins by raman spectroscopy. *Polymer Testing*, 28(1), 42–45.
- O'Brian, D. J., Mather, P. T., & White, S. R. (2001). Viscoelastic properties of an epoxy resin during cure. *Journal of Composite Materials*, 35, 883–904.
- O'Brien, D. J., & White, S. R. (2003). Cure kinetics, gelation, and glass transition of bisphenol f epoxide. *Polymer Engineering and Science*, 43(4), 863–874.
- Philipp, M., Muller, U., Sanctuary, R., Kieffer, J., Possart, W., & Kruger, J. K. (2011). On the interplay between matter transport and structure formation at epoxy-hardener interfaces visualized by scanning brillouin microscopy. *Soft Matter*, 7, 118–124.
- Plepy, A., & Farris, R. (1990). Evolution of residual stresses in three-dimensionally constrained epoxy resins. *Polymer*, 31(10), 1932–1936.
- Plepy, A., Vratsanos, M. S., & Farris, R. J. (1994). Determination of residual stresses using incremental linear elasticity. *Composite Structures*, 27(1–2), 51–56. special issue advances in fiber reinforced composites technology.
- Rabearison, N., Jochum, C., & Grandidier, J. (2009). A fem coupling model for properties prediction during the curing of an epoxy matrix, Proceedings of the 17th International Workshop on Computational Mechanics of Materials – IWCMM-17 . *Computational Materials Science*, 45(3), 715–724.
- Ramakrishnan, B., Zhu, L., & Pitchumani, R. (2000). Curing of composites using internal resistive heating. *Journal of Manufacturing Sciences and Engineering*, 122, 124–131.
- Ramos, J., Pagani, N., Riccardi, C., Borrajo, J., Goyanes, S., & Mondragon, I. (2005). Cure kinetics and shrinkage model for epoxy-amine systems. *Polymer*, 46(10), 3323–3328.
- Revello, M., Saggese, L., & Gaiero, E. (2000). Compression molding of SMCs. *Comprehensive composite materials*. Amsterdam: Elsevier, pp. 763–805.
- Rudd, C. (2001). Resin transfer modeling and structural reaction injection molding. *ASM handbook 21 – Composites*. ASM International.
- Sanctuary, R., Philipp, M., Kieffer, J., Muller, U., Possart, W., & Kruger, J. K. (2010). Trans-interfacial polymerization and matter transport processes in epoxy-alumina nanocomposites visualized by scanning brillouin microscopy. *The Journal of Physical Chemistry B*, 114(25), 8396–8404. PMID: 20521803.
- Shanku, R., Vaughan, J., & Roux, J. (1997). Rheological characteristics and cure kinetics of EPON 862/W epoxy used in pultrusion. *Advances in Polymer Technology*, 16(4), 297–311.
- Song, S., Waas, A. M., Shahwan, K. W., Faruque, O., & Xiao, X. (2008). Compression response of 2D braided textile composites: Single cell and multiple cell micromechanics based strength predictions. *Journal of Composite Materials*, 42(23), 2461–2482.
- Song, S., Waas, A. M., Shahwan, K. W., Faruque, O., & Xiao, X. S. (2009). Compression response, strength and post-peak response of an axial fiber reinforced tow. *International Journal of Mechanical Sciences*, 51(7), 491–499.
- Song, S., Waas, A. M., Shahwan, K. W., Xiao, X., & Faruque, O. (2007). Braided textile composites under compressive loads: Modeling the response, strength and degradation. *Composites Science and Technology*, 67(15–16), 3059–3070.
- Sui, L., Huang, L., Podsiadlo, P., Kotov, N. A., & Kieffer, J. (2010). Brillouin light scattering investigation of the mechanical properties of layer-by-layer assembled cellulose nanocrystal films. *Macromolecules*, 43(22), 9541–9548.
- Varshney, V., Patnaik, S.S., Roy, A. K., & Farmer, B. L. (2008). Molecular dynamics study of thermal transport phenomena in cross-linked polymer: Epon 862 with curing agent W (DETDA). In: 49th Structures, structural dynamics, and materials conference (Shaumburg, IL). AIAA/ASME/ASCE/AHS/ASC.
- White, S., & Hahn, H. (1992). Process modeling of composite materials: Residual stress development during cure. Part I: Model formulation. *Journal of Composite Materials*, 26(16), 2402–2422.
- Wu, J., & Chung, D. (2004). Calorimetric study of the effect of carbon fillers on the curing of epoxy. *Carbon*, 42(14), 3039–3042.
- Yamura, H., Matsukawa, M., Otani, T., & Ohtori, N. (1999). Brillouin scattering study on the elastic properties of epoxy adhesive layer. *Japanese Journal of Applied Physics*, 38(5B, Part 1), 3175–3178.
- Yates, B., McCalla, B. A., Phillips, L. N., Kingston-Lee, D. M., & Rogers, K. F. (1979). The thermal expansion of carbon fibre-reinforced plastics. *Journal of Materials Science*, 14, 1207–1217. doi:[10.1007/BF00561306](https://doi.org/10.1007/BF00561306).
- Yerramalli, C. S., & Waas, A. M. (2002). In situ matrix shear response using torsional test data of fiber reinforced unidirectional polymer composites. *Journal of Engineering Materials and Technology*, 124(2), 152–159.